BSGF - Earth Sciences Bulletin 2021, 192, 15
© P. Perron *et al.*, Published by EDP Sciences 2020
https://doi.org/10.1051/bsgf/2020038

BSGF
Earth Sciences Bulletin
Available online at:
www.bsgf.fr

Open Access

Control of inherited accreted lithospheric heterogeneity on the architecture and the low, long-term subsidence rate of intracratonic basins

Paul Perron[1,2,*], Laetitia Le Pourhiet[2], Michel Guiraud[1], Emmanuelle Vennin[1], Isabelle Moretti[2,3], Éric Portier[4] and Moussa Konaté[5]

[1] Université de Bourgogne Franche-Comté, Centre des Sciences de la Terre, UMR CNRS 6282 Biogéosciences, 6 Bd Gabriel, 21000 Dijon, France
[2] Sorbonne Université, CNRS-INSU, Institut des Sciences de la Terre Paris, ISTeP UMR 7193, F-75005 Paris, France
[3] ENGIE, 1, place Samuel de Champlain, Faubourg de l'Arche, 92930 Paris La Défense, France
[4] NEPTUNE Energy International S.A., 9-11, Allée de l'Arche – Tour EGEE, 92400 Courbevoie, France
[5] Département de Géologie, Université Abdou Moumouni de Niamey, BP 10662, Niamey, Niger

Received: 5 June 2020 / Accepted: 13 September 2020

Abstract – Intracratonic basins tend to subside much longer than the timescale predicted by thermal relaxation of the lithosphere. Many hypotheses have been suggested to explain their longevity, yet few have been tested using quantitative thermo-mechanical numerical models, which capture the dynamic of the lithosphere. Lithospheric-scale geodynamic modelling preserving the tectono-stratigraphic architecture of these basins is challenging because they display only few kilometres of subsidence over 1000 of km during time periods exceeding 250 Myr. Here we present simulations that are designed to examine the relative role of thermal anomaly, tectonics and heterogeneity of the lithosphere on the dynamics of intracratonic basins. Our results demonstrate that initial heterogeneity of accretionary continental lithosphere explains long-term subsidence and the arches-basins architecture of Saharan type intracratonic basins at first order. The simulations show that initially heterogeneous lithospheres inherited from accretion are strong enough to resist local isostatic re-equilibration for very long period of time. Indeed, the lateral density variations store potential gravitational energy that is then slowly dissipated by differential erosion and slow vertical movements. For relatively well-accepted coefficient of erosion of 10^{-6} m^2/s, the subsidence last longer than 250 Myr. Extensional tectonic forcing and thermal anomalies both result in an effective strength drop of the lithosphere, which allows a temporal acceleration of local isostatic re-equilibration. Periodic changes in far field tectonic forcing from extension to compression complicate the tectono-stratigraphic architecture (intra-basin arches, sub-basins) introducing stratigraphic unconformities between different neighbouring basins such as the ones observed in North Africa.

Keywords: Intracratonic basin / heterogeneous accreted mobile belt / isostatic compensation / potential subsidence / gravitational potential energy / far field tectonic / Saharan Platform

1 Introduction

Intracratonic basins also called "cratonic basins", "interior cratonic basins" or "intracontinental sags" host most of freshwater aquifers, minerals resources and hydrocarbon reserves of the world (Allen and Allen, 2013). They have a widespread geographic distribution (see Fig. 6 from Heine *et al.*, 2008) and have in common several features thoroughly reviewed by Allen and Armitage (2011). Here we just summarize them to better define the objects of this study. As their name states, intracratonic basins are located in the interior of continents, far from any active margins (stretched or convergent) upon stable continental lithosphere areas. They are usually large (> 150.00 km^2 in area) circular, elliptical to oval-shaped in plan and saucer-shaped in cross section. Despite their small stretching factors (Armitage and Allen, 2010; Allen and Allen, 2013), they can accumulate large amount of sediments. Their dynamics is characterized by long lasting sedimentation (> 250 Myr) with sublinear to gently exponential shape subsidence curves that corresponds to

*Corresponding author: paul.perron@upmc.fr; paul.perron@hotmail.fr

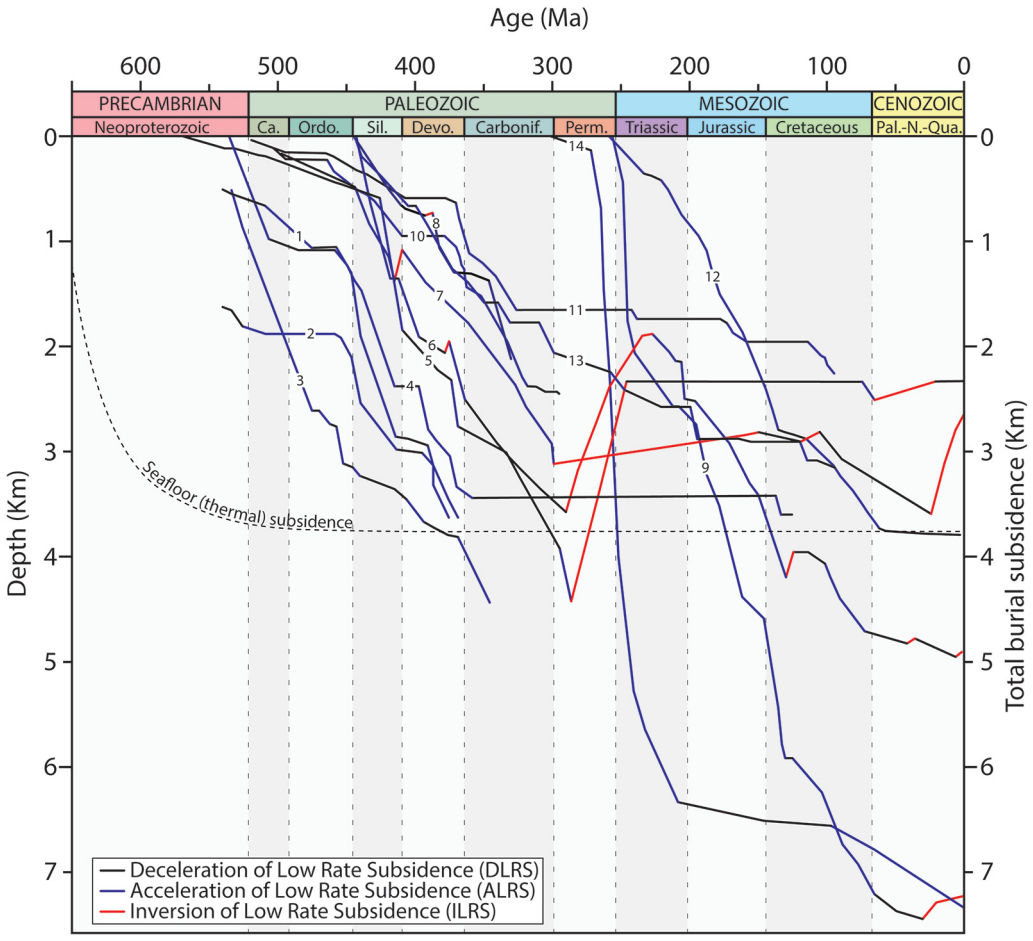

Fig. 1. Compilation of total burial subsidence of intracratonic basins modified from literature showing periods of acceleration (ALRS: Acceleration of the Low Rate subsidence), deceleration (DLRS: Deceleration of the Low Rate Subsidence) and inversion (ILRS: Inversion of the Low Rate Subsidence) of the low rate subsidence. 1: New York, USA, well 7-6 (Adkinson, 1966 from Sleep *et al.*, 1980); 2: Ohio, USA, well 6-6 (Adkinson, 1966 from Sleep *et al.*, 1980); 3: Johnson County, USA, Illinois well (Sleep *et al.*, 1980); 4: Michigan Basin well, USA (Sleep and Sloss, 1978); 5: Ahnet Basin, Algeria, well W1 (Kracha, 2011); 6: Ghadames/Berkine Basin, Algeria (Yahi, 1999); 7: Illizi Basin well, Algeria (Wells *et al.*, 2018); 8: Mouydir Basin, Algeria Well W21 (Perron *et al.*, 2018); 9: Tyumen SG-6 section, Urengoy region, Russia (Nikishin *et al.*, 2002); 10: North Dakota, Williston Basin, USA, well 11 (Smith, 1967 from Fowler and Nisbet, 1985); 11: Williston Basin, Saskatchewan, USA, well 1 (Fowler and Nisbet, 1985); 12: Paris Basin, France, well CFX-1 (Brunet and Pichon, 1982); 13: Parnaíba Basin, Brazil, well 2-BAC (Tozer *et al.*, 2017); 14: Northeast German Basin, Germany (Scheck and Bayer, 1999). The dashed line represents thermal seafloor subsidence from Xie and Heller (2009). For 7 (well W1, Ahnet Basin) and 19 (well W21, Mouydir Basin) see Figure 2 for localisation. Notice that this is a compilation of worldwide intracratonic basins, where different explanations from the literature (*e.g.* Xie and Heller, 2009; Allen and Armitage, 2011) can be invoked to capture the origin of their subsidence.

subsidence rates as low as 5 to 50 m/Myr (Fig. 1). These basins are filled with continental to shallow-water sedimentation indicating low topographic relief. In many cases, their structural framework can be characterized by the association of arches *s.l* and basins of different kilometric wavelengths reactivated through time (de Brito Neves *et al.*, 1984; Quinlan, 1987; Seyfert, 1987; Perron *et al.*, 2018).

Multiple hypotheses and models have been invoked to explain the dynamics of these slow subsiding long-lived intracratonic basins (see Allen and Armitage, 2011 and references therein or Hartley and Allen, 1994). The preservation of the low subsidence rate together with the long exponential decay of subsidence with time (Fig. 1) has led many authors to propose essentially a thermal decay subsidence origin (Haxby *et al.*, 1976; McKenzie, 1978; Nunn *et al.*, 1984; Nunn and Sleep, 1984; Nunn, 1994; Howell and van der Pluijm, 1999; Xie and Heller, 2009; Armitage and Allen, 2010; Holt *et al.*, 2015; Cacace and Scheck-Wenderoth, 2016). However, supposing thermal diffusion, most of the thermal relaxation of the lithosphere should be mainly achieved within the first 50 Myr (Moretti and Froidevaux, 1986; Bond and Kominz, 1991; Fig. 1) and it does not *a priori* explain the long geological time scale (*i.e.* >250 Myr) over which these basins subside. Moreover, thermal relaxation alone does not explain the deviations of the subsidence pattern (also referred as stepwise pattern; Janssen *et al.*, 1995) featured by alternation of periods of quiescence (*i.e.* deceleration; DLRS: Deceleration of the Low Rate Subsidence), acceleration (ALRS: Acceleration of the Low Rate subsidence) and inversion (ILRS: Inversion of the Low Rate Subsidence) of the

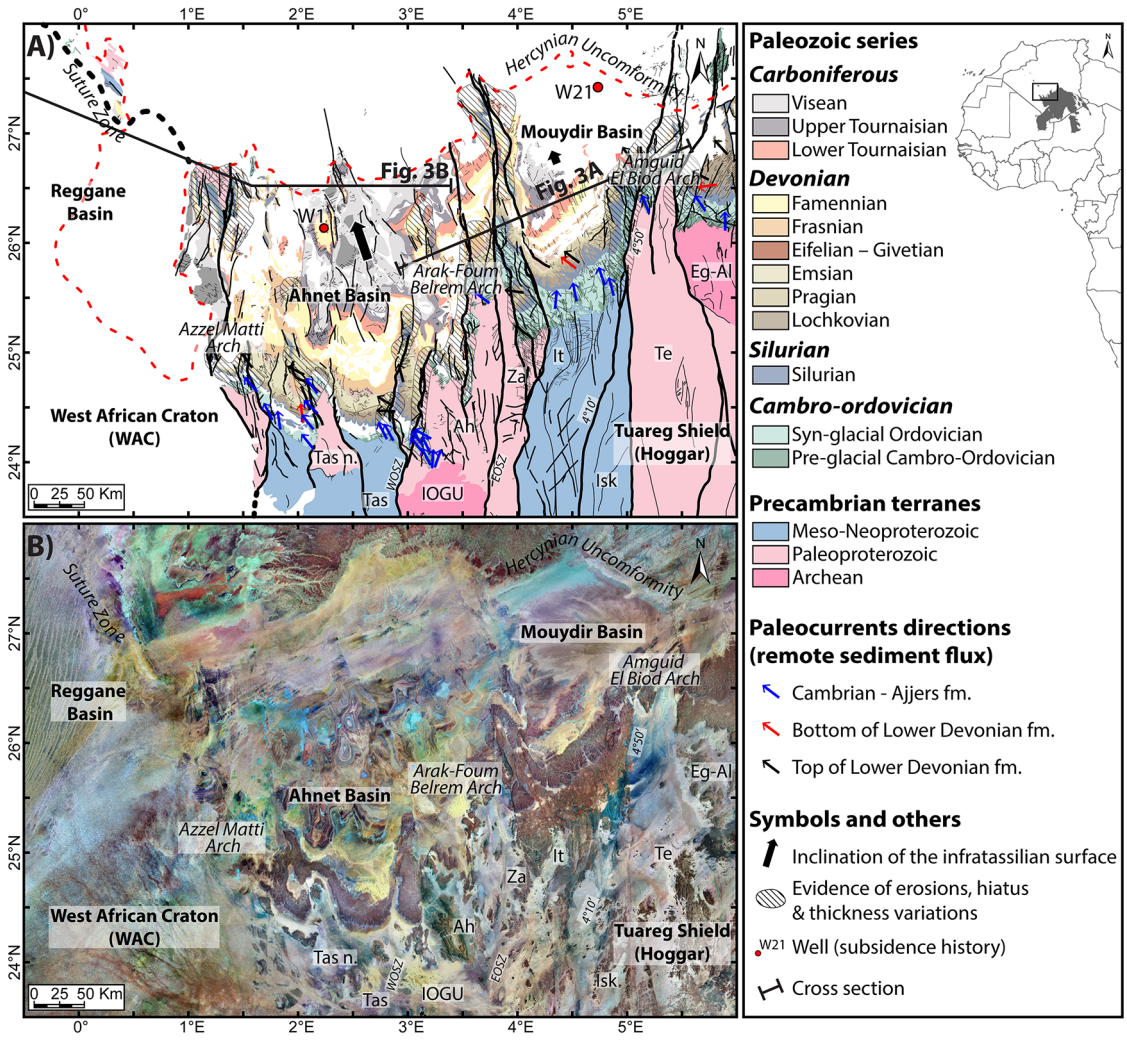

Fig. 2. (A) Geological map of the Ahnet and the Mouydir Basins modified from Perron *et al.*, (2018) showing the specific zonation of the terranes, the paleocurrents directions (from Beuf *et al.*, 1971) and the evidence of sedimentary structures on arches (from Perron *et al.*, 2018; Wendt *et al.*, 2006). Terrane names and abbreviations: Tassendjanet (Tas), Tassendjanet nappe (Tas n.), Ahnet (Ah), In Ouzzal Granulitic Unit (IOGU), In Zaouatene (Za), In Teidini (It), Iskel (Isk), Tefedest (Te) and Egéré-Aleskod (Eg-Al). Shear zone and lineament names and abbreviations: west Ouzzal shear zone (WOSZ), east Ouzzal shear zone (EOSZ), 4°10' shear zone and 4°50' shear zone. B) Satellite images of the Paleozoic series in the Ahnet and Mouydir basin (Landsat 7 ETM + from USGS: https://earthexplorer.usgs.gov/).

subsidence (Fig. 1), which are very well documented on the Saharan Platform (Perron *et al.*, 2018). Driven by this geological example, the present contribution introduces alternative hypothesis to thermal subsidence in context of accretionary lithosphere and aims to test these different hypotheses by the mean of thermo-mechanical simulations in order to circumscribe what first-order mechanisms can maintain the low, long-term subsidence rate of the intracratonic basins through the geological time and what second-order forcing can explain local acceleration and inversion of subsidence.

After presenting the main characteristics of accretionary lithosphere and arch and basin structures that typically form on them, focusing on the Saharan Platform, part 3 outlines our working hypothesis before describing and justifying the adopted modelling scheme. Part 4 and 5 details the results of the simulation in term of subsidence curves and basin architecture. Finally, a ternary classification of intracratonic basins is proposed based on their tectono-stratigraphic architecture. We place the different basins of the Saharan Platform example that inspired this modelling study (Perron *et al.*, 2018; Figs. 2 and 3) into this new classification to discuss what the tectonic architecture of basins tells us about external and internal forcing that are responsible for their long subsidence histories.

2 Arches and basins in accretionary type lithosphere: the Saharan Platform example

Intracontinental sag basins (Holt *et al.*, 2010, 2015; Holt, 2012) are often basins formed upon a heterogeneous inherited lithosphere assembled during different former geodynamic events (Condie, 2007; Cawood, 2009; Cawood *et al.*, 2009) very long time before they begin to subside (Allen and

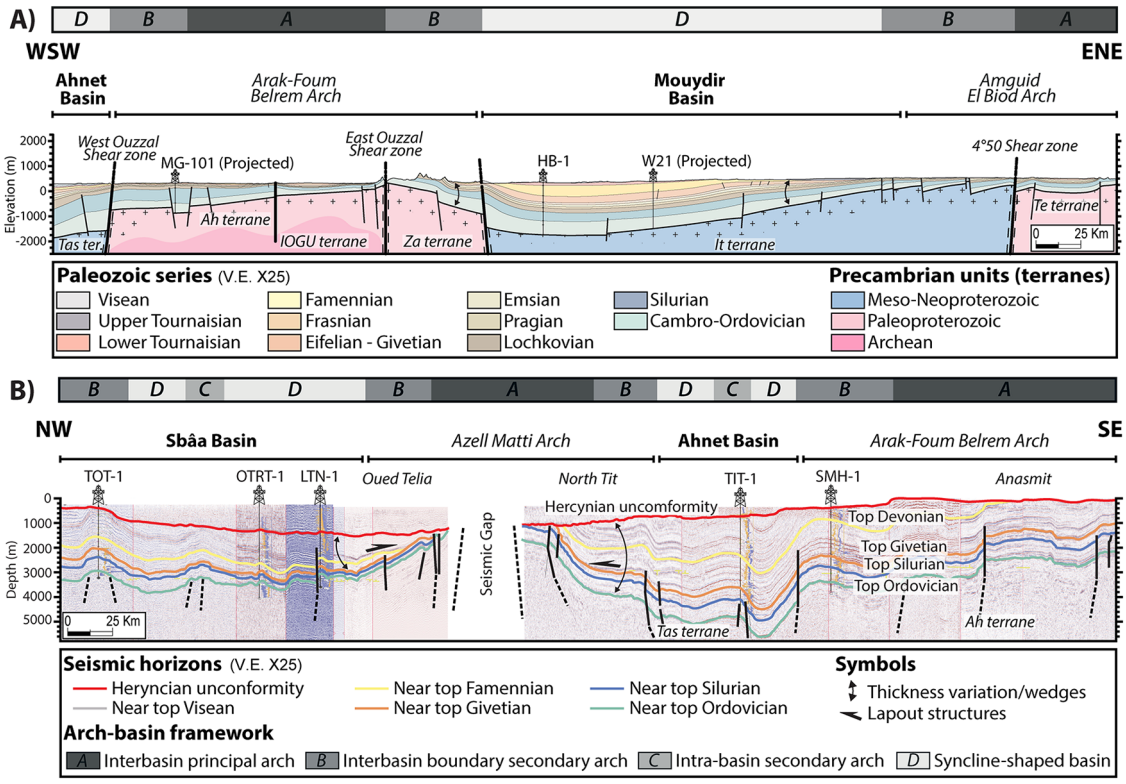

Fig. 3. (A) WSW-ENE geological cross section of the Mouydir Basin showing typical arch and basin architecture defined as a syncline-shaped basin with boundary secondary arches. (B) NW-SE seismic profiles of the Ahnet Basin defined as a complex shaped basin with intra-basin arches. The specific zonation of the terranes age with the arches-basins architecture is observed (see also Perron *et al.*, 2018).

Armitage, 2011). Among them, accretionary type lithospheres are the result of the orogenic collage of different types of lithosphere that occurred during the Archean and Proterozoic time (de Wit *et al.*, 1992). These ultra-hot and accretionary orogens differs from modern ones (Chardon *et al.*, 2009; Cagnard *et al.*, 2011) in the sense that accretion occurs along sub-vertical shear zones rather than mega-thrust observed in contemporary orogens. Evidence of heterogeneous segmentations of cratons are documented in the world such as in Africa (Hartley *et al.*, 1996; Hartley and Allen, 1994; Fishwick and Bastow, 2011; de Wit and Linol, 2015; Brahimi *et al.*, 2018), Russia (Cherepanova *et al.*, 2013; Cherepanova and Artemieva, 2015), in North-America (Lyatsky *et al.*, 2006; Eaton and Darbyshire, 2010; Frederiksen *et al.*, 2013; Tesauro *et al.*, 2015; Caravaca *et al.*, 2017; Daly *et al.*, 2018), South-America (Chernicoff and Zappettini, 2004; Mantovani *et al.*, 2005; Heilbron *et al.*, 2008; Bologna *et al.*, 2013; Daly *et al.*, 2014, 2018; Tozer *et al.*, 2017), and Asia (Ratheesh-Kumar *et al.*, 2014). According to many authors (de Brito Neves et al., 1984; Caravaca *et al.*, 2017; Daly *et al.*, 2018; Peace *et al.*, 2018; Perron *et al.*, 2018; Phillips *et al.*, 2018), these basement inherited heterogeneities (*i.e.* terranes) separated by shear zone are essential ingredients of the formation of arch and basin features, constraining their shape and architecture through time. While many studies stress the importance of the vertical shear zones in the basement on structural framework developed later on (*e.g.* Célérier *et al.*, 2005; Audet and Bürgmann, 2011; Tesauro *et al.*, 2012; Perron *et al.*, 2018), the collided terrains that typically constitute cratonic areas also display difference in crustal thickness, lithology and geochemical content that should result in different rheological behaviour (Djomani *et al.*, 2001; Artemieva and Mooney, 2002; Artemieva, 2009; Cherepanova and Artemieva, 2015).

The Saharan Platform presents probably one of the rare well-documented example of intracratonic basins in the world where, thanks to recent flexural uplift (Rougier *et al.*, 2013), both the nature of basement and the sedimentary architecture are directly outcropping (Figs. 2 and 3) and can be correlated with seismic and well data. In this area, the terranes have been accreted together during the Eburnean (~2 Ga) and the early Pan-African (~850 Ma) orogeny; (Bertrand and Caby, 1978; Black *et al.*, 1994) long before the Cambrian (540 Ma), which corresponds to the onset of their subsidence (Allen and Armitage, 2011). Geological/geophysical observations of the Hoggar Massif (Bouzid *et al.*, 2008; Brahimi *et al.*, 2018; Perron *et al.*, 2018), where terranes structures are exhumed and outcropps (Fig. 2) indicate the existence of mainly sub-vertical sutures and shear zones of lithospheric scale between terranes of different nature (*e.g.* Liégeois, 2019). These studies also give an approximative idea of the various dimensions of these terranes (Bouzid *et al.*, 2008; Liégeois *et al.*, 2005; Brahimi *et al.*, 2018).

Focusing on the Mouydir and the Ahnet Basins, Figures 2 and 3 permits to illustrate the concepts of basins and arches through simple syncline-shaped basins and a more tectonised complex-shaped basins. In both cases arches correspond to condense sedimentary series located upon "old" Archean and Paleoproterozoic age terranes while the depocenters rest on

younger Proterozoic domains (Perron *et al.*, 2018). This typical tectono-stratigraphic architecture in basins and arches (also referenced as paleo-highs) was also described in this area by Eschard *et al.* (2010).

In both cases, the paleocurrent directions are globally oriented NNW which is more or less parallel to the major lineaments (Beuf *et al.*, 1971). However, local variations of these directions can be observed during Cambro-Ordovician, Caledonian tectonics pulses (*e.g.* Beuf *et al.*, 1968; Fig. 2A). They can be punctually oriented orthogonally to the main directions. These variations evidence that both a remote sediment supply from upstream and a punctual local erosion/deposition processes during uplift of arches (*i.e.* Archean terranes) are active.

During the Paleozoic, the structures of these basins are mainly controlled by N-S sinistral or dextral high dip ($> 60°$) normal faults (*i.e.* transtension to transpression) forming horst and graben network associated with forced folds (Fig. 3) weakly inverted and/or reactivated through time (see tectonic history and stresses orientation in Zazoun, 2001; Haddoum *et al.*, 2001; Perron *et al.*, 2018). This structural framework of the sedimentary cover is preferentially nucleated on the basement structures (Perron *et al.*, 2018; Figs. 2 and 3) which are characterized by lithospheric shear zones with predominantly higher dip (Bouzid *et al.*, 2008; Brahimi *et al.*, 2018). Yet, the tectono-thermal intensity in the Ahnet Basin was more significant than elsewhere on the Saharan platform because it was relatively close to the deformation front of the Hercynian orogeny and the West African Craton suture (Fig. 2A; Boote *et al.*, 1998; Logan and Duddy, 1998; Haddoum *et al.*, 2001; Zazoun, 2001; Coward and Ries, 2003; Akkouche, 2007; Craig *et al.*, 2008). The global syncline-shaped tectono-stratigraphic architecture (1st order pattern) best illustrated in the Mouydir Basin (syncline-shaped basin type; Fig. 3A) can be complexified by the presence of interbasin/intrabasin secondary arch structures (2nd order pattern) observed in the Ahnet Basin (complex-shaped basin type; Fig. 3B). The thickness reaches 1.7 to 7.1 km in the Ahnet Basin which is in average higher than the Mouydir type basins (Beuf *et al.*, 1971; Conrad, 1984; Wendt *et al.*, 2006, 2009; Zieliński, 2012).

3 Working hypotheses for modelling

3.1 Key observations and questions

From the observations listed above, arches and basins structures can be formed above heterogeneous lithosphere separated by vertical mega shear zones. As many modelling studies implies that strength contrast between blocks is often more likely to be reactivated than fault zones (Ranalli, 2000; Buiter and Pfiffner, 2003; Le Pourhiet *et al.*, 2004; Heron *et al.*, 2016; Lafosse *et al.*, 2016; von Tscharner *et al.*, 2016) whether this inheritance recorded in the sedimentation of the basin is related to the weakness of the shear zones or to the rheological contrast between Archean and the Proterozoic lithospheres remains an open question.

Aside from the compositional and mechanical heterogeneities, we cannot *a priori* disqualify the potential effect of regional thermal events that could affect old accretionary lithosphere, yet, it is legitimate to assume that the geometry predates any destabilizing thermal event related to subsidence. Nevertheless, while slow exponentially decaying subsidence is often attributed to thermal relaxation, other diffusive processes such as erosion and sedimentation would result in similar signature but with different rates. It is therefore important to quantitatively test the effect of slowly decaying thermal anomalies *versus* surface processes on subsidence pattern for different thermo-rheological structures.

Finally, the contrast observed between simple syncline-shaped basins (*e.g.* Mouydir Basin) and complex-shaped basins (*e.g.* Ahnet Basin) seems to be related to far field tectonics solicitation of the system. The sediment routing in the basin highlights that this local tectonic activity is related to change in sources of sediments. Whether these phenomena are first or second order players in the long-term subsidence of basin and arch structures is unknown. While it is always possible to focus on one explanation using oversimplified models, here we have chosen to test the relative importance of all these parameters and their non-linear feedbacks using thermo-mechanical simulations.

3.2 General model set up

In order to test the influence of structural inheritance, thermal perturbations, far field tectonics and sediment supply on the subsidence of intracontinental basins, we use thermo-mechanical simulations. The model domain is 300 km deep and 1600 km long. The mesh is refined towards the surface to enable modelling large-scale dynamics over 250 Myr with a resolution of 500 m at the surface in reasonable computing time. This surface resolution allows us to visualize and constrain the tectono-stratigraphic architecture of the synthetic basins. Appendix A details how conservations of momentum and energy are solved numerically together with surface process evolution.

All the models use a free upper boundary surface subject to erosion–sedimentation allowing the development of sedimentary basins. These surface processes are modelled using Culling's (1965) law with a constant diffusivity (κe) of $1.10^{-6}\,m^2 \cdot s^{-1}$ which account for local erosion/deposition processes. All the models have the same thermal boundary conditions. Temperatures are fixed at the top and base of the model to 0 °C and 1400 °C respectively, and a null heat flux is assumed on the model lateral boundaries (Fig. 4C). The 300 km model domain thickness permits to limit artificially plate growth by conduction to 275 km depth without modelling the whole mantle convection. This boundary condition is similar to the finite plate approximation that is used for oceanic plate geotherms (Parsons and Sclater, 1977).

3.3 Structural inheritance

In order to measure the effect of structural inheritance on subsidence, we compare models with laterally homogeneous composition (P and A) with a model M that is largely inspired from the geodynamic setting of the Saharan platform (Perron *et al.*, 2018) where both the age (correlated to the density of the lithosphere) and the geometry of different terranes control the architecture of the basins and arches (Figs. 2 and 3). Geophysical observations in the area (Bouzid *et al.*, 2008; Liégeois *et al.*, 2005; Brahimi *et al.*, 2018), have also

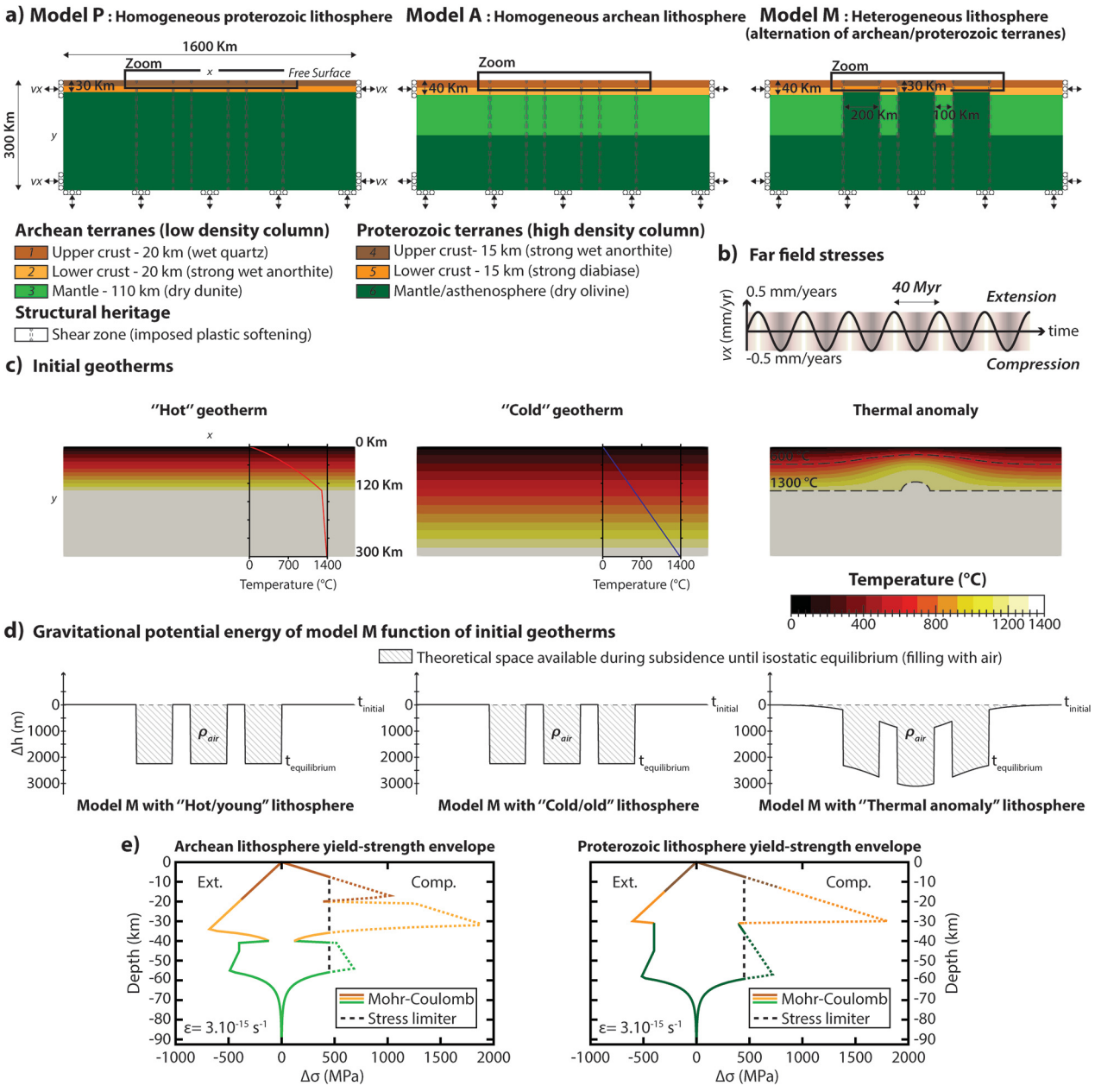

Fig. 4. (A) Inputs models (model P, A and M) of the different simulations with the different parameters applied in experiments such as (B) the far field stresses (sinusoidal extension-compression 40 Myr) and (C) initial temperatures of the lithosphere (thermal anomaly, "hot" and "cold" geotherms). (D) Gravitational potential energy: Theoretical space available for the basin subsidence according to local isostatic equilibrium of model M for each different initial geotherms (basins filled with air). (E) Yield-strength envelopes (Mohr-Coulomb representation) for Archean and Proterozoic lithosphere with a "Hot" geotherm calculated for a strain rate of $3.10^{-15}\,s^{-1}$ and a stress limiter at 450 MPa (value from Watremez *et al.*, 2013). $\Delta\sigma$ represents the deviatoric stress, positive values under extension and negative values under compression.

contributed to define the dimensions of model M (*i.e.* size of terranes and shear zones).

This model consists of three 200 km wide Proterozoic terranes separated by two Archean terranes of 100 km in width sandwiched in between two 400 km wide Archean cratons (Fig. 4A). In order to measure the relative effect of weak shear zones *versus* contrasting rheological profile on inheritance, all the models, A P and M includes weak 2 km wide vertical shear zones affected with a friction of 0.01 and a cohesion of 10 MPa.

The Archean terranes have a 40 km thick crust (20 km quartz dominated upper crust +20 km anorthite dominated lower crust) and a lighter mantle lithosphere that reflects their high magnesium number. The Proterozoic terranes have a 30 km thick crust (15 km quartz dominated upper crust +15 km pyroxene dominated lower crust) and their mantles have the

Table 1. Rheological parameters used in all experiments. References are from R & D (Rybacki and Dresen, 2000), G & T (Gleason and Tullis, 1995), C & T (Carter and Tsenn, 1987), G & E (Goetze and Evans, 1979) and M (Mackwell *et al.*, 1998). Other parameters described in Appendix A, which have fixed values, are listed here: $\alpha = 3.10^{-5}\,K^{-1}$ (thermal expansion), $\beta = 1.10^{-11}\,Pa^{-1}$ (adiabatic compressibility), $\kappa_e = 1.10^{-6}\,m^2\,s^{-1}$ (erosional diffusive coefficient), $\kappa = 1.10^{-6}\,m^2\,s^{-1}$ (heat diffusivity), $\varepsilon_{min} = 0$, $\varepsilon_{max} = 1$, $Cp = 1000\,J\,kg^{-1}\,K^{-1}$ (heat capacity), $H = 3.10^{-9}\,W\,kg^{-1}$ (heat production).

	Archean upper crust	Archean lower crust	Archean Mantle	Proterozoic upper crust	Proterozoic lower crust	Mantle	Sediments	Units
Phase	1	2	3	4	5	6	7	
Lithology	Wet quartz	Strong wet anorthite	Dry dunite	Strong wet anorthite	Strong diabase	Dry olivine	Wet quartz smaller friction	
n	4	3	3.5	3	4.7	3	4	
A	$1.1.10^{-4}$	$4.0.10^{2}$	$4.85.10^{4}$	$4.0.10^{2}$	8	$7.0.10^{3}$	$1.1.10^{-4}$	$MPa^{-n}.s^{-1}$
Q	223	356	535	356	485	510	223	$kJ \cdot mol^{-1}$
ρ_0	2800	2900	3335	2900	2900	3345	2400	kg/m^3
φ_0	30	30	30	30	30	30	30	°
φ_∞	10	10	10	10	10	10	10	
Co_0	20	20	20	20	20	20	20	MPa
Co_∞	1	1	20	1	10	20	1	MPa
References	G & T	R & D	C & T	R & D	M	G & E	G & T	

same reference density as the asthenosphere. The rheological parameters of the Archean and Proterozoic lithosphere are compiled in Table 1. Notice that these parameters are not constrained by xenoliths data from the Saharan Platform due to their lack. However, they stay coherent with global examples of Archean and Proterozoic lithospheres (*e.g.* Djomani *et al.*, 2001; Artemieva and Mooney, 2002; Artemieva, 2009). The strength of the lithospheric mantle is limited to 450 MPa (*i.e.* stress/viscosity limiter) to mimic dislocation glide and Peierls creep (which is not implemented here). The value is chosen according to Watremez *et al.* (2013) who calibrated the maximum strength of the Arabian mantle using the topography of the Gulf of Aden.

3.4 Thermal perturbations

The "cold" lithosphere corresponds to the steady state solution of the heat equation for the boundary conditions imposed on our 300 km thick modelling domain and the 1300 °C isotherm often referred as thermal lithosphere asthenosphere boundary is located at 270 km depth. It is similar to the solution of a finite plate cooling model with radiogenic heat production (Turcotte and Schubert, 2014), assuming 300 km plate thickness as the maximum thickness for continental lithosphere and a 1400 °C basal temperature.

Nevertheless, although these basins are currently located on stable shields, we cannot disregard that the system may have been out of thermal equilibrium at the onset of subsidence. We therefore design models with homogenously "hot" geotherm that are coherent with the model of Holt *et al.* (2010) and with a lithosphere having undergone an orogenic cycle (Beuf *et al.*, 1971; Guiraud *et al.*, 2005) and models with localised "thermal anomaly" that are intended to explore the effect of more localised thermal subsidence related to deep thermal events which could correspond to igneous activity observed for example on the Saharan platform, (*e.g.* Liégeois *et al.*, 1991; Moreau *et al.*, 1994; Derder *et al.*, 2016; Perron *et al.*, 2018). The "hot" and "temperature anomaly" models are designed with non-steady state initial conditions using Burov and Diament (1995) analytical solution for finite plate cooling including radiogenic heat production decreasing from a surface value of $3.10^{-9}\,W\,kg^{-1}$ with a characteristic exponential decay of 10 km. This analytical solution accepts two parameters: 1) a plate thickness and 2) a thermal age which are usually interpreted as due to the last tectono-metamorphic event. The heat production imposed in the sediments is $1.10^{-9}\,W\,kg^{-1}$, a non-null value motivated by the singular presence of (organic-rich) "hot shales" identified in the North Africa (Lüning *et al.*, 2000, 2003). In the "hot" lithosphere models, we use set the 1300 °C isotherm at 120 km and use a thermal age of 400 Myr. For the "thermal anomaly" models, the thermal age follows a Gaussian distribution in x-axis (abscissa) from 50 Myr at the centre of the model to 400 Myr on the borders with a standard deviation of 600 km (Fig. 4C). In both cases the initial geotherm is prolongated down to 300 km where temperature reaches 1400 °C using a constant linear gradient (~0.5 °C/km). During the simulations, these thermally young lithospheres can be destabilized convectively (usually in the initial stages) but more generally, they cool down over time by conduction until they reach a steady state temperature that corresponds to the "cold" lithosphere initial geotherm.

3.5 Sediment routing and far field tectonics

In some models, we also add a source term in the Culling model that corresponds to remote sediment supply (equivalent to regional source) by drainage network that runs perpendicular to the cross-section of the model (see Jourdon *et al.*, 2018 for implementation and discussion).

The vertical boundaries of the model have null vertical shear stress. Horizontal kinematic boundary conditions (Fig. 4A) are either zero or their integral with time is zero. This second type of boundary conditions is used to simulate the

Table 2. List of parameters inputs for each model. Note that duration of all models is 250 Myrs. TA: Thermal anomaly initial geotherm; HL: "Hot" initial geotherm; "Cold" initial geotherm. M5', M7', and M7 models are presented in Supplementary Data.

Models	Lithosphere type	Far field stresses (compression/extension alternation)	Initial geotherms type	Remote sediment supply
A1	Homogeneous archean	No	TA	No
A2	Homogeneous archean	Yes	HL	No
P1	Homogeneous proterozoic	No	TA	No
P2	Homogeneous proterozoic	Yes	HL	No
M1	Heterogeneous archean/proterozoic	No	TA	No
M2	Heterogeneous archean/proterozoic	Yes	HL	No
M2'	Heterogeneous archean/proterozoic	Yes	CL	No
M3	Heterogeneous archean/proterozoic	No	HL	No
M3'	Heterogeneous archean/proterozoic	No	CL	No
M4	Heterogeneous archean/proterozoic	Yes	TA	No
M5	Heterogeneous archean/proterozoic	No	HL	Yes
M5'	Heterogeneous archean/proterozoic	No	CL	Yes
M6	Heterogeneous archean/proterozoic	Yes	TA	Yes
M7	Heterogeneous archean/proterozoic	Yes	HL	Yes
M7'	Heterogeneous archean/proterozoic	Yes	CL	Yes

effects of far field orogenic cycle. A sinusoidal variation with time period of 40 Myr peak to peak has been chosen as representative between two shortening events (Fig. 4B). This regular cyclicality of far field tectonic loading is a rough approximation/simplification for the different pulses of extensional and compressional tectonics that have affected the Saharan platform (Ziegler *et al.*, 1995; Coward and Ries, 2003; Perron *et al.*, 2018). The very small velocity *vx* applied on the boundary, *i.e.* ± 0.5 mm/Myr ($1.5\,e^{-11}$ m.s^{-1}) at peak, ensures a minimal amount of shortening and stretching per cycle (10 km over 1600 km). In order to compensate for stretching and shortening, a small velocity (6*vx*/16, *i.e.* ± 0.2 mm/yr at peak) is applied at the base of the model to ensure the volume of the modelling domain remains constant. This value together with the size of the model domain corresponds to background strain rate of 10^{-17} s^{-1} that is considered as rigid plate on the world strain-rate map (Kreemer *et al.*, 2014).

4 Accretionary *vs* homogeneous lithosphere

In this part, after briefly describing the results of the simulation with homogeneous Archean (model A) and Proterozoic (model P) lithosphere structured by an imposed tectonic heritage (4.1), we will concentrate on characterizing how the initial geotherm (4.2), far field tectonic forcing (4.3) and interplay between the two (4.4) are recorded in accretionary type of lithosphere (model M). The input parameters for each model (A, P and M) are referenced in Table 2.

4.1 Limits of homogeneous lithosphere

The main purpose of the experiments presented in Figure 5 is to show that homogeneous Archean or Proterozoic lithospheres affected by weak vertical shear zones do not produce intracratonic basins when submitted to thermal anomaly (A1 and P1, Fig. 5) nor far field tectonics (A2 and P2 Fig. 5).

On the one hand, thermal anomaly alone (P1 and A1 in Fig. 5) results in a complete lack of deep sedimentary basins after 250 Myr. The subsidence rate displays an exponential decay that is characteristic of thermal subsidence. In both simulations, the subsidence actually ceases after 150 Myr (see W1-P1 and W1-A1 in Fig. 6). On the second hand, the two homogeneous models submitted to far field tectonic loading display small basins that are controlled by the presence of the imposed pre-existing faults. In both cases, the faults, despite their weakness, are not reactivated in a strict sense. Instead, they help initiating new dip slip faults. During the extension phases Archean and Proterozoic terranes have similar thermo-rheological structure, *i.e.* crust and mantle are coupled and brittle, and four narrow basins are formed. Yet basins are wider in the Archean than in the Proterozoic terranes because they root slightly deeper according to the rheology of the lithospheric mantle. During compression however, the thick Archean crust displays a decollement at the mid-crust that is not present in the Proterozoic lithosphere (see yield-strength envelope, Fig. 4E). This induces a different mechanical response. The Proterozoic lithosphere deforms preferentially on the inherited weak zones splitting the extensional basin in two sub-basins (P2, Fig. 5) while the Archean upper crust pops up along the dip-slip faults (A2, Fig. 5). In these two runs, the maximum of strain (and of basin thickness) is concentrated along the second shear zone from the limits of the models.

The subsidence curves show a linear decreasing trend with alternation of up and down deviations of amplitude of 110 m for P2 and 400 m for A2 (Fig. 6). The Figure 7 aims to analyse the behaviour of accretionary lithosphere (model M) in response to initial geotherm and tectonic loading. It clearly evidences that all the models displayed capture the first order feature of low rate intracontinental basins unlike the experiments shown in Figure 5. A subtle difference between homogeneous models and heterogeneous ones is the location of active faults when loaded by tectonics. All models with

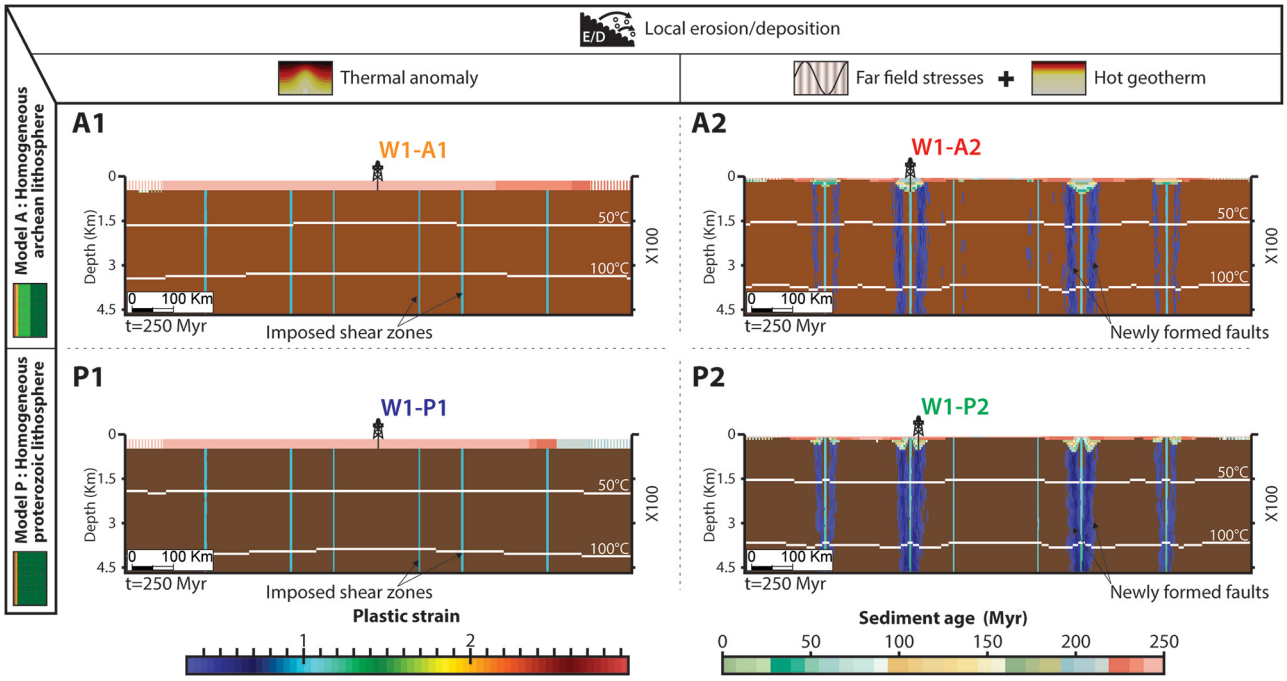

Fig. 5. (A1) Model A with thermal anomaly shows no creation of basin. (P1) Model P with thermal anomaly shows no creation of basin. (P2) Model P with far field stresses shows the creation of eights narrow basins with chaotic stratigraphic architecture near shear zones. (A2) Model A with far field stresses displays the formation of four narrow basins with chaotic stratigraphic architecture above shear zones.

accretionary lithosphere and without remote sediment supply (Fig. 7) display larger basins on the sides of the model domain than in the centre. In contrast, models with homogeneous lithosphere (A2 and P2 in particular) display larger fault displacement in the centre of the domain. The reason for this contrasting behaviour is the known positive feedback between sedimentation and fault activity (*e.g.* Beaumont *et al.*, 1992; Burov and Poliakov, 2001; Jourdon *et al.*, 2018). The presence in the model M domain of large stable and buoyant Archean cratonic areas located on either side of the heterogeneity provides the lateral basins with an extra source of sediments that does not exist in model P2 and A2 (*i.e.* Proterozoic and Archean homogeneous lithospheres with tectonics and only local erosion/deposition). A more obvious difference between the homogeneous lithosphere models displayed in Figure 5 and the heterogeneous ones displayed in Figure 7 is of course the presence of intracratonic basins separated by arches of Archean lithosphere. Consequently, the rest of this contribution will focus on model M that is a mechanically heterogeneous accretionary lithosphere.

4.2 Impact of initial geotherm

The first line of Figure 7 represents a "hot" lithosphere which can cool down with time (M2 and M3 in Fig. 7), the second one a thermally equilibrated "cold" (M2' and M3' in Fig. 7), and the last one is a "hot" lithosphere affected by an initial thermal perturbation (M1 and M4 in Fig. 7) that could be related to igneous activity.

The experiment M1 (*i.e.* heterogeneous lithosphere with a thermal anomaly and local erosion/deposition) displays three bowl-shaped basins created upon the 3 Proterozoic terranes, in our configuration *i.e.* two peripheral basins and one central basin, separated by basement inter-basin arches upon Archean terranes (Fig. 7). The peripheral basins are 200 km wide and 1.25 km deep. The central basins are thinner (*i.e.* 0.8 km) and narrower (*i.e.* 140 km) than peripheral ones.

During the simulation, due to the relief creation, the uplifted Archean terranes get eroded and sediments deposited upon Proterozoic ones. No sediment is deposited on Archean terranes (*i.e.* arches). The basins form topographic lows, which indicate that sedimentation rate does not compensate for the creation of accommodation space. The basins are starved. The thickness of the different sedimentary layers increases towards the centre of the basins and decreases progressively approaching the arches, forming growth strata. Truncations (M1 in Fig. 7) show that the strata are successively eroded before the next deposits. Consequently, the width of the basins remains stable through time.

For each model with the "cold" lithosphere inputs (model M2' with tectonics and M3' without tectonics in Fig. 7), the major trends of the architecture described previously remain identical. Nevertheless, the thickness of the different basins is smaller than in models with an initially "hot" lithosphere (M1 and M3 in Fig. 7). The maximum of thickness of model M3' (*i.e.* "cold" heterogeneous lithosphere with only local erosion/deposition) reaches 1.1 km, which is 300 m less than the model M3 (*i.e.* "hot" heterogeneous lithosphere with only local erosion/deposition). The analysis of subsidence curves between model M3' and M3 shows more or less a same trend with a shift of 300 m at the end of the 250 Myr (W1-M3' and W1-M3 in Fig. 8).

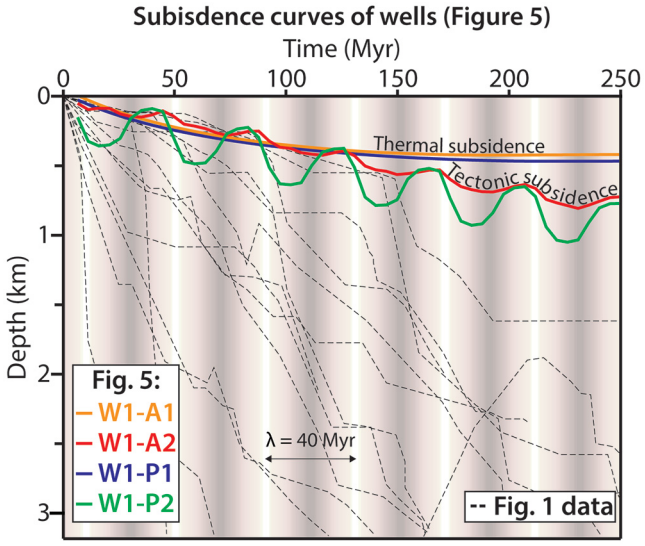

Fig. 6. Subsidence curves from different models in Figure 5 (wells W1-A1 to W1-A2 and W1-P1 to W1-P2) associated with Figure 1 bibliographic data (dashed lines). The thermal subsidence of W1-A1 and W1-A2 is achieved after 150 Myr. The wells P1 and P2 show linear decay subsidence with deviations of different amplitudes. See Figure 4B for the boundary conditions.

We have shown that thermal anomaly below homogeneous lithosphere (model P and A) cannot explain the long-lived subsidence of intracratonic basins (1st order pattern) and whatever the characteristics of the lithosphere. In less than 150 Myr the equilibrium is reached (see dotted lines W1-A1 and W1-P1 in Fig. 8). On the contrary, with a heterogeneous lithosphere formed by the accretion of different terrains of different densities, the morphology of the curve (see W1-M1 in Fig. 8) indicates that the subsidence, in that case related to buried loads, is still active after 250 Myr. Besides, this part shows that there is no relevant control of initial geotherm on the 1st order subsidence pattern of intracratonic basins (M1, M3 and M3' in Fig. 8).

4.3 Impact of far field stresses (tectonics)

The purpose of this second part is to analyse the behaviour of the three types of lithosphere in response to far field tectonic periodic loading by comparing simulation P2, A2 (i.e homogeneous lithospheres; Fig. 5) and M2 (*i.e.* heterogeneous lithosphere; Fig. 7).

The accretionary lithosphere model M2 (*i.e.* "hot" heterogeneous lithosphere with tectonics) display the formation of arches and basins, which are very similar at first order to the structural pattern obtained with simulation M1 (*i.e.* heterogeneous lithosphere with thermal anomaly; Fig. 7). At second order, some dissimilarities are however to be noted. The bottom of the saucer-shaped basins of M2 is flat, with angular shape and with some weak undulations that do not happen in the purely thermally-driven model (M4 in Fig. 7). Also, the main basins are formed in peripheral positions rather than in the centre of the heterogeneous corridor.

This second part demonstrates that for similar tectonic loading, homogenous lithosphere with faults remain stable, and only allows the formation of small basins at the apex of the shear zones (*i.e.* the imposed structural heritage). Their subsidence curves display a linear trend with deviations (W1-A2 and W1-P2 in Fig. 6). Heterogeneous lithosphere on the contrary forms basin and arch structures associated to inherited lithospheric heterogeneities in buoyancy and rheology that are very similar to the results obtained with a thermal anomaly. The far field stresses trigger period of acceleration, deceleration and inversion of the subsidence (W1-M2 in Fig. 8) that were identified on the data displayed in Figure 1 (2nd order signal). It also complicates the architecture of intracratonic basins.

4.4 Interplay between tectonic and thermal anomalies

Having shown that basins and arches only form and last for long in case of heterogeneous lithosphere, we now want to evaluate the relative effect of thermal anomaly and far field tectonics on the location and rate of subsidence. This third part therefore aims (1) to dissociate the role of the thermal anomaly from the role of heterogeneous lithospheric column, (2) understand the interplay between tectonic and thermal anomaly using two extra experiments M3 and M4. The M3 model does not include any thermal anomaly nor tectonic forcing, the M4 model at the opposite includes a thermal anomaly and a tectonic forcing. Both models are displayed in Figure 7 together with M1 and M2.

After 250 Myr, M3 simulations show globally the same features as M1 (Fig. 7). The peripheral basins are 200 km wide and 1.5 km deep. The central basins are thinner (*i.e.* 1 km) and narrower (*i.e.* 160 km) than peripheral ones. This peculiarity can be explained by the larger surface of erosion of the two Archean blocks at the ends of the models (*i.e.* the source of sediments is more important) directly feeding the peripheral basins (*i.e.* sedimentation rate varying according the different basins) and by the thermal doming of the central basin due to the initial thermal anomaly. The starving of sediments in the central basin could be seen as an effect of the 2D model approach. The only difference between these two models is indeed a negative vertical shift of 125 m of subsidence curve of M3 as compared with M1 (W1-M3 and W1-M1 in Fig. 8) that we interpret as initial thermal doming in M1.

After 250 Myr, M2 and M4, the two models subjected to tectonic forcing display more differences than M1 and M3 (Fig. 7). While M2 displays the same overall distribution of depocentres as M1 and M3 and only differs by the flat angular base of the basins, M4 displays more complex distribution of depocentres. Central and boundary sub-basins are indeed separated by inter-basin arches, inter-basin arches secondary arch and intra-basin secondary arches. This specific structural framework has been described in Perron *et al.* (2018). Moreover, the maximum of deformation is localized in the peripheral basins for M2 and in the central basin, above the initial thermal anomaly, for M4 (Fig. 7).

The secondary arches and basins are controlled by steeply dipping conjugated normal faults (synthetic and antithetic), forming graben structures located from either side of terranes boundaries (and shear zones; M4 in Fig. 7).

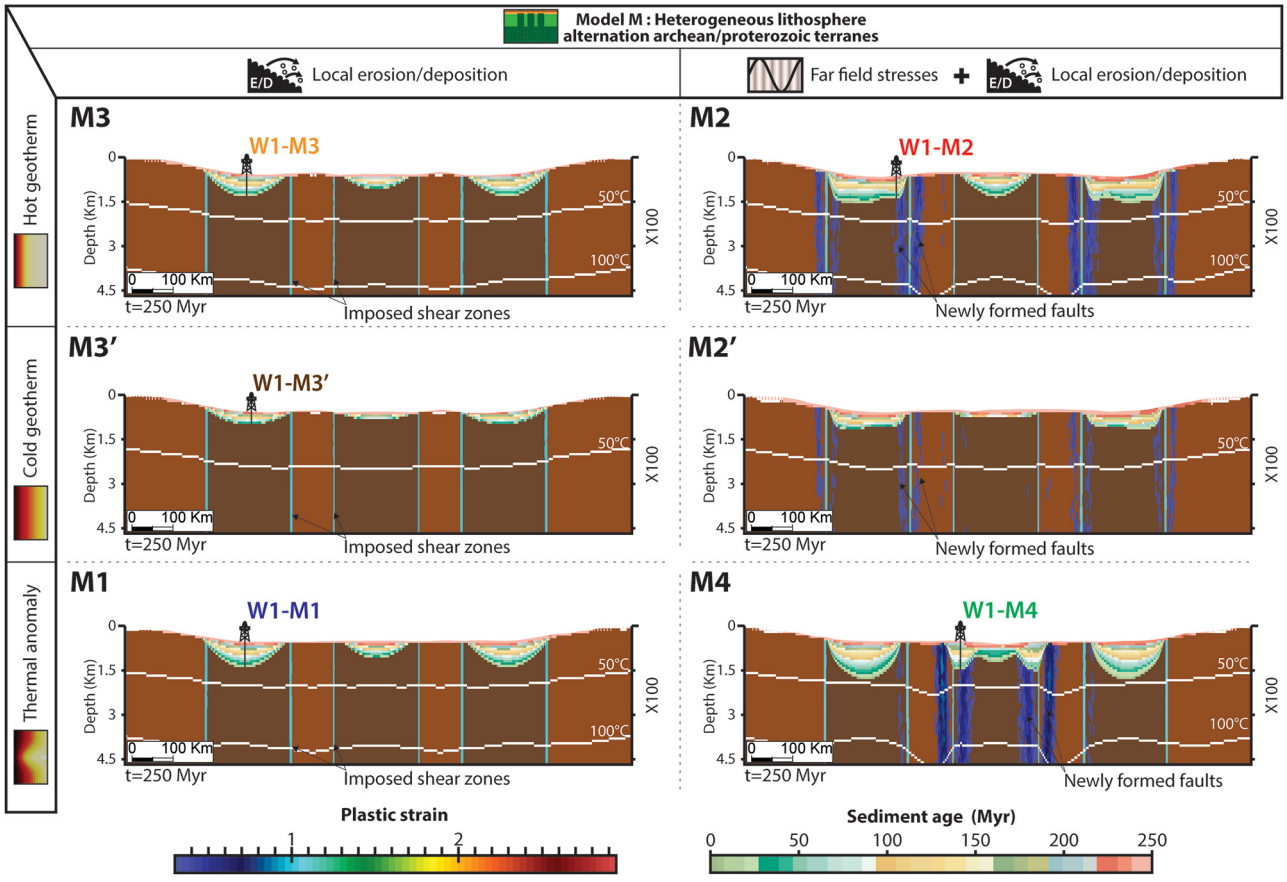

Fig. 7. (M1) Model M with thermal anomaly displays the creation of arches and basins architecture (*i.e.* One central basin and two peripheral basins separated another by arches). (M3) Model M without thermal anomaly shows the same architecture of basins than M1 demonstrating the minor influence of thermal anomaly. (M2) Model M with far filed stresses and without thermal anomaly modifies peripheral basins structural architecture by flattening the bottom. (M4) Model M with far field stresses and thermal anomaly modifies central basin structural architecture (*i.e.* formation of grabens above the shear zones). (M2') and (M3') are featured by an initial "cold" geotherm while the other by an initial "hot" geotherm.

These structures are repeatedly activated and re-activated during extensions and inversed during compressions due to far field tectonics (*i.e.* sinusoidal boundary conditions). The comparison between M2 (*i.e.* "hot" heterogeneous lithosphere with tectonics) and M4 (*i.e.* heterogeneous lithosphere with thermal anomaly and tectonics; Fig. 7) demonstrates that the thermal anomaly favours the formation of new faults in the early stage of the simulation. Fault softening allows continuous activity after the thermal anomaly dissipation. The presence of thermal anomaly is recorded by higher strain intensity in the basins that are located above them. Thermal weakening of the lithosphere indeed reduces the thickness of the effective brittle layer and the integrated strength of faults is reduced as their surface diminishes. The subsidence curves are so impacted and show a linear decreasing trend with alternation of up and down deviations of amplitude of 280 m for M2 and 960 m for M4 (W1-M2 and W1-M4 in Fig. 8). The deformation as well as the amplitude of deviations are much more significant above the central thermal anomaly.

The comparison of these four tests (Fig. 7) clearly indicates that slow isostatic rebalancing by differential erosion between different accreted terranes with heterogenic rheological properties (Archean and Proterozoic) can be considered as a driving force for the creation of accommodation. Thermal or tectonic forcing are not necessary conditions for the creation of basins and their preservation through time. However, while thermal forcing alone does not induce very large changes in the distribution and shape of the basins, tectonic forcing is sensitive to the presence of thermal anomalies.

5 Architecture of basins in accretionary lithosphere

5.1 Covering the arches: Impact of remote sediment supply

One may note that none of the simulations present sediments covering the arches, as it is the case in the sub-Saharan platform (Fig. 3; Perron *et al.*, 2018). As surface processes permit the local isostatic re-equilibration and controls it (M3 in Fig. 7), we expect that variations in remote sediment supply implemented as a source term might also affect the subsidence of the basins and arches. Thus, we

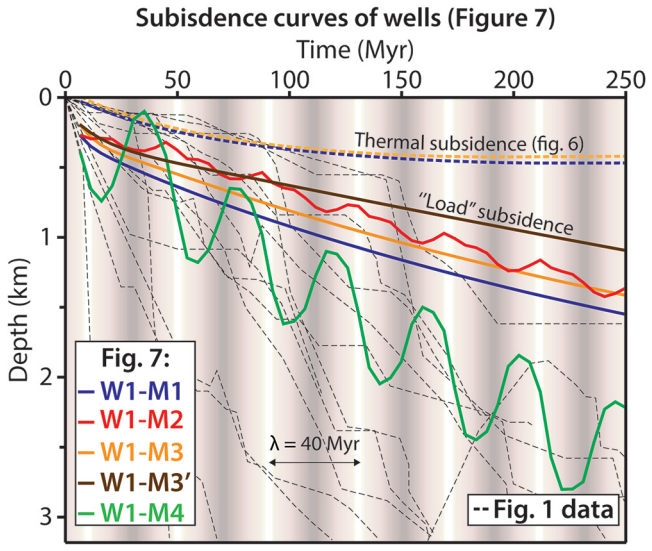

Fig. 8. Subsidence curves from different models in Figure 7 (wells W1-M1 to W1-M4) associated with Figure 1 bibliographic data. The subsidence of W1-M1, W1-M3 and W1-M3' is constant after 250 Myr (*i.e.* still have a potential of subsidence), in contrast with the subsidence of W1-A1 and W1-A2 where it stops after 150 Myrs. The wells W1-M2 and W1-M4 show linear decay subsidence with deviations of different amplitude. See Figure 4B for the boundary conditions.

compare the basins obtained with a heterogeneous lithosphere (model M) without remote sediment supply (*i.e.* only local sediment supply by diffusive erosion/deposition processes; M3 in Fig. 7) to a model with remote sediment supply (M5 in Fig. 9; see also Fig. 10 for comparison between these two models).

After 250 Myr, we observe the same configuration than the last simulations (M1 and M3 in Fig. 7). The peripheral basins are characterized by a thickness of 3 km and the central basin by a thickness of 2.75 km. Contrary to all previous models, we observe now the presence of sediments on arches up to about 1.5 km thick. The width of the peripheral basins is about 350 km and 300 km for the central one (from the edge to the centre of the arches). The curves display an exponential decay trend and almost reach equilibrium after 250 Myr (Fig. 9C). They show a differential subsidence between peripheral (W1), central basins (W3) and arches (W2). The average rate of subsidence is 12 m/Myr in peripheral basins (W1), 11 m/Myr in the central basin (W3) and 6 m/Myr on arches (W2).

During the simulation, the Proterozoic terranes and the Archean terranes are differentially subsiding one relative to each other. The addition of remote sediment supply increases the temperature of the basins. The temperatures of the basins in simulations of Figure 7 are < 50°C and > 100 °C in Figure 9A (see also Fig. 10). We observe an unexpected rise up of the isotherms under Proterozoic terranes (*i.e.* basins) and a go down under Archean terranes (*i.e.* arches). It is caused by the slow burial of the radiogenic heat production of the basement that follows the relative uplift of the Archean terranes regarding the Proterozoic terranes (Fig. 10). This phenomena is discussed by Sandiford and McLaren (2002).

The analysis of these two simulations M3 (*i.e.* "hot" heterogeneous lithosphere with only local erosion/deposition) and M5 (*i.e.* same as M3 with remote sediment supply in addition) shows the importance of remote sediment supply rate as a forcing factor on the dynamics and filling of basins (Fig. 10). This parameter also reveals the limits of 2D modelling. Adding more sediments than what is eroded allows to rapidly reach the isostatic compensation by increasing the subsidence rate. It also brings sediment on arches and enlarges the width of the basins. The stratigraphic structures (*e.g.* onlaps and erosional truncations) upon the arches allow us to understand the complexity of the sedimentary history of the basin.

5.2 More complex models

We have now circumscribed the first-order trend controlling the low long-lived subsidence rate and the architecture (arches and basins) of the intracratonic basins. Besides, the second-order trend featured by deviations with periods of acceleration, deceleration and inversion of the low subsidence rate can be explained by far field stresses alternating compressional/extensional pulses (*i.e.* changes in tectonic processes occurring at the adjacent plate margins). We now want to compare the results at smaller scale by comparing the internal architecture of M5 (Fig. 9), a simple model driven by buoyancy and erosion with remote sediment supply, to M6 (Fig. 11), the same model submitted to both thermal anomaly and tectonic forcing.

In M5, the association of arches and basins (Fig. 9A) is evidenced by divergent onlaps (*i.e.* growth strata), truncations and reduced thicknesses when approaching the arches (*i.e.* Archean terranes). The stratigraphic succession is featured by many hiatuses that can be followed on the model at the local scale (one basin) and the regional scale (three basins). The unconformities are particularly well marked on arches where some entire stratigraphic units are missing or are amalgamated. Besides, some stratigraphic units are present in central basin and not in peripheral basins. The differential movement of the basement caused by the relative uplift of the Archean terranes ("lighter") regarding the Proterozoic terranes ("heavier") is at the origin of these observed sedimentary structures (truncations, hiatus and divergent onlaps) near the arches (Figs. 9A and 9B).

Simulation M6 (*i.e.* heterogeneous lithosphere with thermal anomaly, remote sediment supply and tectonics; Fig. 11) displays the same sub-basins and sub-arches than M4 (*i.e.* heterogeneous lithosphere with thermal anomaly and tectonics), with more sediments due to remote sediment supply. The left peripheral basin and the central basin are both characterized by a thickness of 4.8 km while the right peripheral one is slightly less thick (4.25 km). We observe the presence of sediments on arches about 2.2 km thick. The maximum of thickness is reached in the central boundary basin which is nearly 5 km thick. The initial thermal perturbation favours the accumulation of more strain on the normal faults that control the central basin. This faster rate of frictional softening is responsible for asymmetrical shape to the central basin (Huismans and Beaumont, 2002) that is not as marked in simulations performed without initial thermal perturbation.

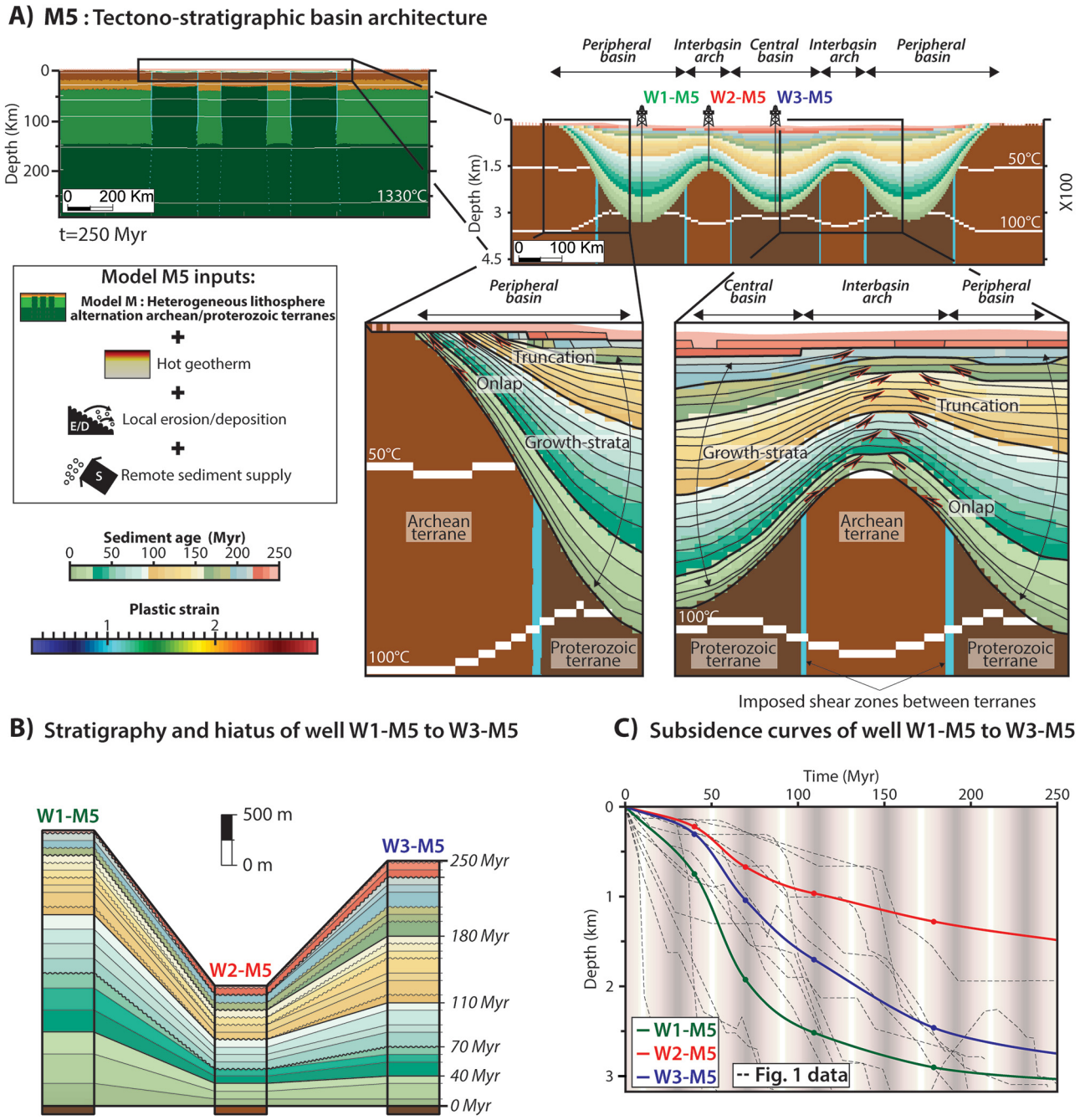

Fig. 9. (A) Tectono-stratigraphic basin architecture and heat production of Model M5 without thermal anomaly shows stratigraphic features (*i.e.* onlaps, truncations and thickness variations) when approaching the arches. (B) Stratigraphy and hiatus repartition between the wells W1-M5 to W3-M5. (C) Subsidence curves of well W1-M5 to W3-M5 are characterized by exponential decay shape. Comparison with Figure 1 subsidence bibliographic data (dashed lines).

The basins display divergent onlaps (*i.e.* growth strata), truncations and reduction in thickness when approaching the different arches (*i.e.* inter-basins or intra-basins on Fig. 11A). The stratigraphic succession features many unconformities. Some entire stratigraphic units are missing in the sub-basins, intra-basin arches and inter-basin secondary boundary arches while present in others (Fig. 11B). The minimum of thickness and the maximum of amalgamated erosional surfaces are detected on the inter-basin principal arches (W5 in Fig. 11). In the central boundary basins (W2 in Fig. 11A), unconformities are observed in the depocentre (maximum thickness recorded in the model) where a continuous conformable stratigraphy would have been expected. It is worth to notice these differences between the basins in terms of truncations and missing series even though the boundary conditions are the same.

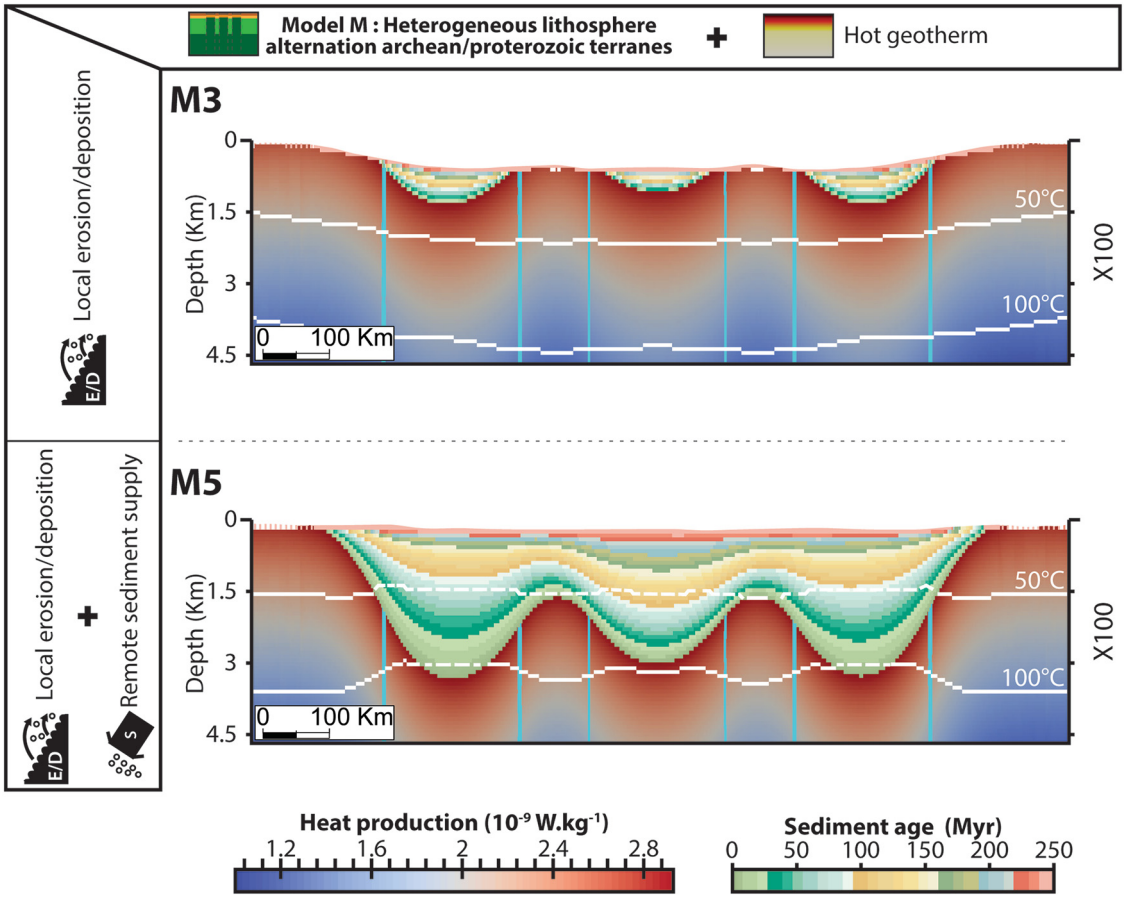

Fig. 10. Comparison between model M3 and M5 showing increase of basin depths and the deposits on the arches in case on higher sediment supply due to remote sediment supply. One may note also that the temperature in the basin and in the crust is affected by this higher sedimentation rate, it is due to heat production of the basement. The isotherms rise up below the basins and down below the arches.

5.3 Basins evolution: key to deciphering past geodynamics

The far field stresses associated with thermal perturbation parameters bring specificities on the tectono-stratigraphic architecture of the basins (Fig. 11). The arch and basin structural first-order pattern (Fig. 9) is remodelled by the formation of grabens near terrane boundaries during extension, they are inverted during compression. It is defined by sub-basins, intra-basin arches and inter-basin secondary boundary arches a characteristic identified in the Saharan intracratonic basins (Perron *et al.*, 2018).

In our case, the lithospheric heterogeneities associated with newly created faults on weakness zones by far field stresses control the compartmentalization and the tectonic kinematics. This individualization of the different structural units and the disparate propagation of the deformation through them explain the diachronic features in the subsidence signal (*i.e.* acceleration, deceleration and inversion) and the stratigraphic succession architecture between neighbouring basins. For instance, we have highlighted that the layers present in the footwall can be eroded in the hanging wall where the maximum of thickness is usually expected.

First of all, the analysis of 1D well burial history shows that, the initial rate of subsidence in the centre of the basins is greater in models with tectonics (W1-M6, 4 and 6 in Fig. 11C) than in models without far field tectonics (W1-M5 and 3 in Fig. 9C). Nevertheless, a clear tectonic signal is only recorded in the sedimentary architecture of the central basin at the onset of the models with tectonics. The peripheral basins do subside faster, but they do not display large temporal oscillations with 40 Myr cycle before 80 Myr. We infer that this delay reflects the reduced strength of the lithosphere at the apex of the thermal anomaly at the onset of the model. When the thermal signal disappears, after 80 Myr, tectonic deformation tends to distributes itself more equally across the three basins.

This suggests that variations of the sedimentary record of tectonic oscillation in subsidence rate is a good indicator for lateral variations in strength of the lithosphere and that whether these variations are stable or not in time can be interpreted as local thermal (non-stationary) or chemical (stationary) weakening of the lithosphere. In other words, the analysis of the subsidence curves (W1-M6 to W4-M6 in Fig. 11C) shows how the far field stresses and thermal anomaly reduce the strength of the lithosphere. Indeed, models without these forcing parameters have basins with less subsidence (*e.g.* W1-M5 in Fig. 9C *vs* W4-M6 in Fig. 11C).

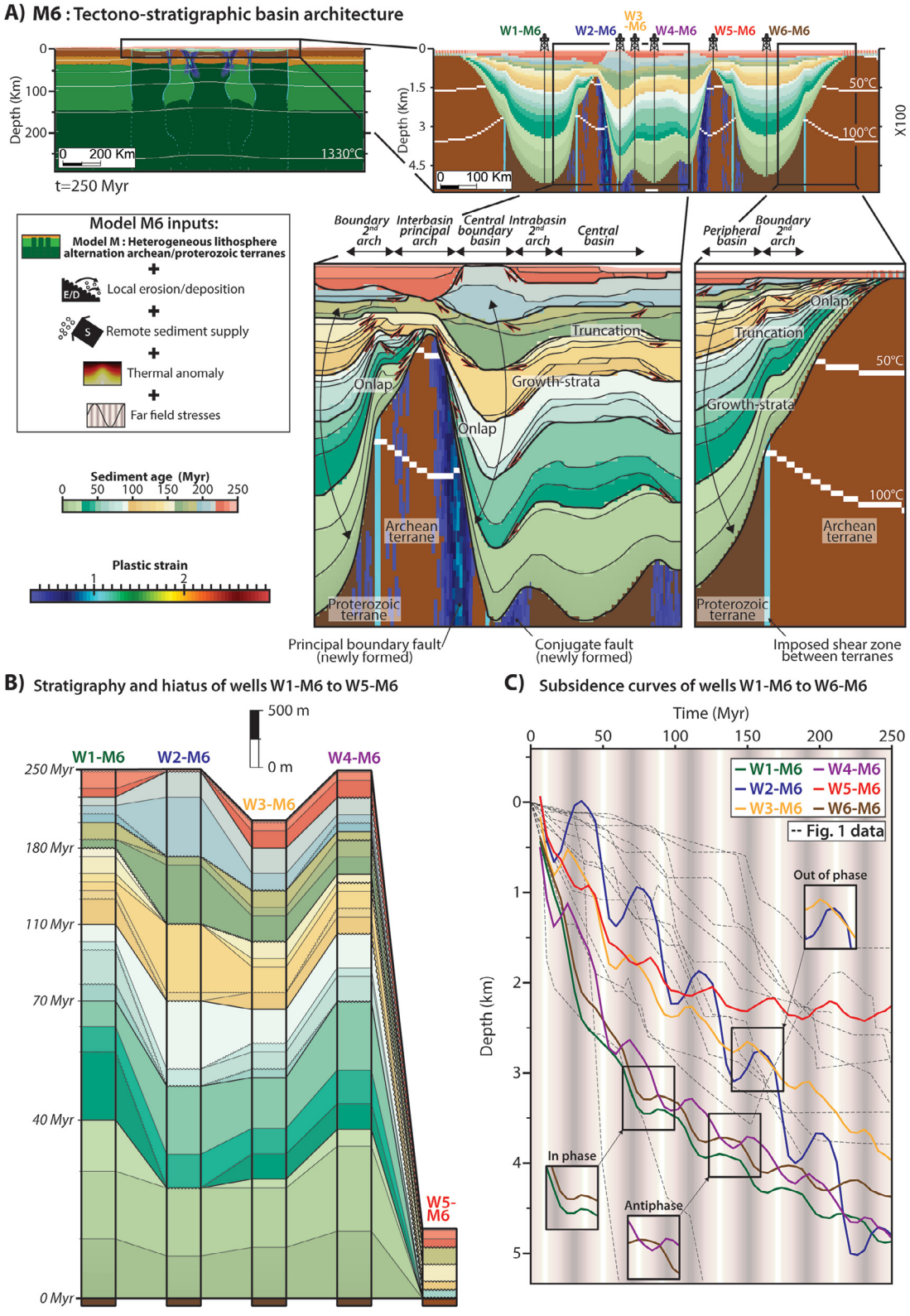

Fig. 11. (A) Model M with far field tectonics, remote sediment supply and thermal anomaly shows a complexification of the basin and arch architecture within Figure 9 with the set-up of inter-basins boundary secondary arches and intra-basin secondary arches. The strain is concentrated in the central basin with creation of grabens above shear zones (*i.e.* limits of terranes). (B) Stratigraphy and hiatus repartition between the wells W1-M6 to W5-M6. (C) Subsidence curves of wells W1-M6 to W6-M6 display an exponential decay with deviations of different amplitude depending on their localization (*i.e.* near maximum strain zones or not). Oscillations related to tectonic loading might be in phase, in antiphase or out of phase between arches and basins or between neighbouring basins but also depending on tectonic context. Comparison with Figure 1 subsidence bibliographic data (dashed lines). See Figure 4B for the boundary conditions.

Looking in more details at the sedimentary record of the far field tectonic sinusoidal loading, it is clear that the subsidence curve response is (1) not always sinusoidal and (2) different whether the wells are located on interbasin principal arches (W5-M6, Fig. 11A), intra-basin arches (W3-M6, Fig. 11A), central boundary basins (W2-M6, Fig. 11A), central basins (W4-M6, Fig. 11A) or peripheral basins (W1-M6 and W6, Fig. 11A).

First of all, tectonic loading is stronger in the well located in central boundary basins (W2-M6, Fig. 11C) than in any other well. At first order, these basins subside rapidly during extension and uplift in lesser amount during compression. In the details the phases of subsidence last longer than the phases of uplift. Indeed, subsidence starts during the slowing down of far field compression and last to the very end of the extension cycle. It is easier to understand how the system behaves by studying the effect of one tectonic cycle (see M6 movie in Supplementary Materials).

The peripheral basins display very short periods of uplift, which corresponds to (1) maximum subsidence rate in the central boundary basins, (2) a marked increase in subsidence rate in the central basin, (3) maximum uplift of arches and (4) onset of subsidence in the central boundary basins. This short period of time corresponds to the period during which extension rate increases at the boundary. During that time period, the system behaves like a rift bordered by the external normal faults of the central boundary basins and where the arches and the peripheral basins behave like uplifting rift shoulders. As extension decelerates at the boundary, the central boundary basins (W2-M6) continue to subside until extension ceased but the outer part of the system relaxes as shown by the subsiding trend of the arches (W5-M6) and the peripheral basins (W1-M6). The central basin (W4-M6) continues to subside at smaller rate than the central boundary basin (W2-M6), which highlights that the conjugate normal faults are still active.

At the onset of compression, the peripheral basin (W1-M6) subsidence accelerates while the central basin (W4-M6) and the central boundary basin (W2-M6) mark a rapid uplift. This corresponds to a phase of tectonic inversion of the principal boundary faults. At the peak of compression, central basin and the central boundary basins start to subside together with the peripheral basins marking the end of tectonic activity on faults for the tectonic cycle. During that phase, the system in buckling down as a whole.

In summary, the principal faults that bounds the central basins are active through all the extensional phases, regardless the rate, but the activity of the conjugate faults starts only towards the peak of extension rate. During compression, principal boundary faults are only active during the phase of shortening acceleration. After the peak of compression, the system is locked and responds by downward buckling of the whole lithosphere. This asymmetric behaviour between extension and compression phase is well explained by the fact that the lithosphere is stronger in compression than in extension (Brace and Kohlstedt, 1980). These delays in inversion of the fault system *versus* global buckling may explain why during the single tectonic event, both extensional or compressional structures can be locally identified in the different sub-basins (see Fig. 17 in Perron *et al.*, 2018).

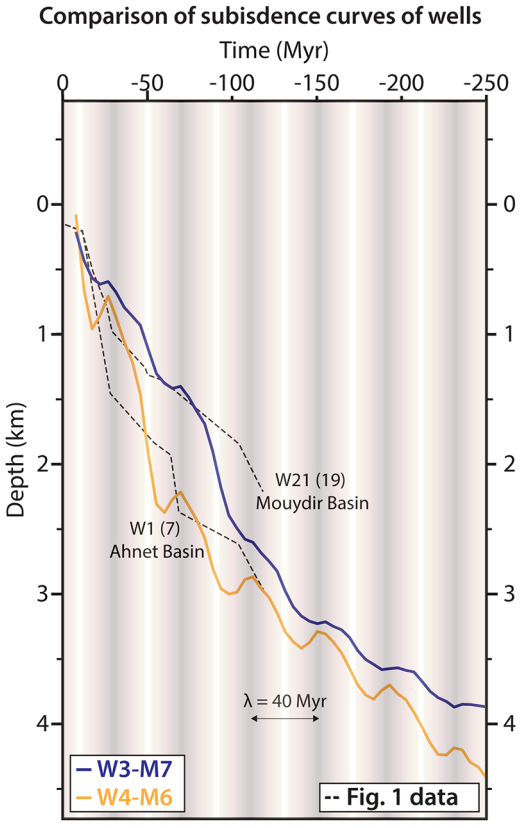

Fig. 12. Comparison of total subsidence curves between numerical models and geological data extracted from the Mouydir Basin, Algeria (9: Well W21; Perron *et al.*, 2018) and the Ahnet Basin, Algeria (5: well W1, Kracha, 2011). The Algerian wells are localized in Figure 2A. The curves are presented in Figure 1.

6 Discussion

6.1 new genetic classification of arch and basin system

While most previous models have considered mainly large-scale geodynamic processes occurring in the lithosphere and did not account for the peculiar architecture and intrinsic characteristics of the sediments filling these basins, our study shows that the local differential strength between the terranes permits to build the complexity recorded in the stratigraphic record.

Based on the simulations, we propose a ternary classification of intracontinental basins that relates basin architectures to three forcing parameters: remote sediment supply, far field tectonics and local thermal perturbation (Fig. 13). A best match with geological data (tectono-stratigraphic architecture and subsidence curves) of Saharan intracratonic basins with the results of models can be proposed and plot on that ternary classification (Fig. 13).

We can observe a particularly good fit of the Mouydir Basin (syncline-shaped basin type; Figs. 2 and 3A and see well W21 in Fig. 12) with the geometry of the peripheral or central basins in the numerical model M7 coupling lithosphere heterogeneity, local erosion/deposition processes, tectonics

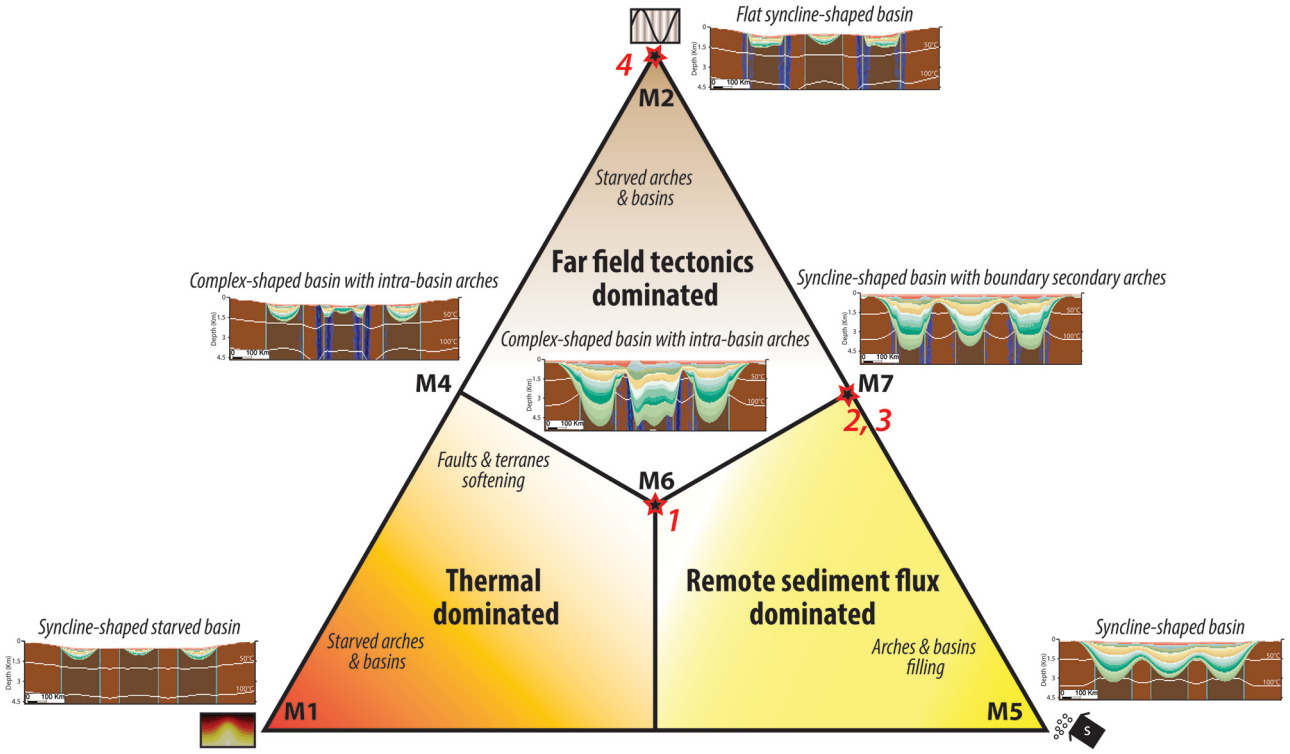

Fig. 13. Ternary classification of low rate intracratonic basins. The diagram relates typical tectono-stratigraphic basin architecture (flat syncline-shaped, syncline-shaped or complex-shaped basin) to internal and external forcing parameters. Example of plotted basins according to their architecture, geometry and subsidence history (see Fig. 12): 1: Ahnet Basin, North Africa (Perron *et al.*, 2018); 2: Mouydir Basin, North Africa (Perron *et al.*, 2018); 3: Tim Mersoï Basin, North Africa (Perron, 2019); 4: Tamesna Basin, North Africa (Lessard, 1961; Perron, 2019). Notice that here the "hot" geotherm (Fig. 4C) is by default if it is not specified. Basic local erosion/deposition processes are active in each model.

and remote sediment supply (see plot in Fig. 13). Conversely, the data from Ahnet Basin (complex-shaped basin type; Figs. 2 and 3B and see well W1 in Fig. 12) better fits with the model M6 which assumes lithospheric heterogeneities, local erosion/deposition processes, tectonics, remote sediment supply and thermal anomaly (see plot on Fig. 13). Modeling infers that tectonic forcing can explain the differences in architecture between the two neighboring basins of Ahnet and Mouydir. According to this same procedure of classification, we can plot in Figure 13 other intracratonic basins of the Saharan Platform (*e.g.* Tamesna and Tim Mersoï Basins).

Upon tectonic forcing, localized vertical movements accommodate basins creation not only by flexure but also by buckling (in compression) or normal faulting (in extension). During extensional events, localized displacements occur along normal faults which do not correspond to vertical weakness zones in the initial geometry. During compressive events, after a short phase of partial inversion of the normal faults, the system locks and weaker ribbons of lithosphere are lifted up by buckling as suggested by many authors (Lambeck, 1983; Cloetingh *et al.*, 1985; Cloetingh, 1986, 1988; Klein and Hsui, 1987; Xie and Heller, 2009). However, buckling instabilities described in these studies are short lived (see also Cloetingh and Burov, 2011), and our proposition to alternate them with period of extension as the advantage of capturing the full complexity of the stratigraphic record. The presence of local and short-lived thermal anomaly in the lithosphere is found to favour faults activity. Here we show that far field stress forcing allows explaining the second order trend characterized by the subsidence deviations pattern and complexification of the structural framework (2nd order pattern). The variations in subsidence rate related to tectonic in our models (Figs. 8 and 11C) are coherent with the data range provided by the literature (Fig. 1).

6.2 Gravitational potential energy: a driver for long-term subsidence?

Several studies have attempted to explain the subsidence at low rate for a long duration (1st order subsidence pattern) of intracratonic basin using classical models (McKenzie, 1978). Alternative models involve cooling following a compressional phase (McKenzie and Priestley, 2016) or mantle delamination (Avigad and Gvirtzman, 2009). The last category involve cooling and thickening of the lithosphere (Holt *et al.*, 2010, 2015) sometimes accelerated by phase transitions in the mantle lithosphere (Naimark and Ismail-Zadeh, 1995; Baird *et al.*, 1995; Hamdani *et al.*, 1991; Kaus *et al.*, 2005; Eaton and Darbyshire, 2010; Gac *et al.*, 2013). Here, we find that thermal anomalies alone do not produce the first order characteristics of basins and arches framework but that contrast in rheologies and densities of Archean and Proterozoic terranes (all M models) are actually necessary and sufficient to drive slow long-term subsidence observed in intracratonic basins (1st order subsidence pattern). The values of subsidence rate in our models (Fig. 8) are coherent with the range of data provided by the literature (Fig. 1).

The main driver of long-term subsidence is therefore stored gravitational potential energy inherited from variation in densities between heterogeneous lithospheric columns. Using the initial variation in thickness and density it is possible to determine an isostatic potential for subsidence (Supplementary Data 1). It is interesting to find out that after 250 Myr none of our simulations ever reach the 5 km sedimentary thickness predicted analytically. With large additional remote sedimentary supply, the models reach regional isostatic equilibrium for less than 3 km of sediments in the basins (M5 in Fig. 9) unless tectonic forcing disrupts the strength of the lithosphere (M6 in Fig. 11). This is consistent with the preservation of gravity anomalies related to change in basement lithologies that is observed today in intracratonic area where adjacent columns of Proterozoic and Archean lithospheres are not yet locally isostatically compensated (Gwavava *et al.*, 1996; Perron *et al.*, 2018). These isostatically uncompensated ancient mass excess can also be related to ancient rift zone (DeRito *et al.*, 1983) or dense body in the lower crust (Haxby *et al.*, 1976; Nunn and Sleep, 1984; Howell and van der Pluijm, 1990, 1999) acting as buried loads. The strength of the lithosphere resists to local isostatic readjustment causing downward surface flexure of the lithosphere that is proportional to the buried load. Our simulations show that erosion and sedimentation dissipate this potential energy by redistributing and slowly dissipating the gravitational potential energy stored by these buried loads. It is beyond the scope of this study to discuss the general hypothesis that models should always start at isostatic equilibrium but out studies show that even with very weak vertical shear zones, in initially "hot" lithosphere, the strength of the lithosphere is sufficient to freeze gravitational potential for uplift and release this energy over long time period. The preservation of subsidence over long time scale in our model is the result of local isostatic re-adjustment to erosion/denudation of uplifted reliefs and deposition in depressions (Avouac and Burov, 1996). This process is time dependant because internal loading is modified through time by erosion. As erosion and sedimentation are diffusive processes just like thermal relaxation, the computed subsidence curves can be described approximately by exponential decay. Our model implies that the decay observed in nature is more sensitive to the rate of basin infilling rather than erosion as high sedimentation rates indeed correspond to faster decay (Fig. 9C).

7 Conclusions

Through a 2D thermo-mechanical modelling, we have applied internal (initial geotherm, far field stresses) and external forcing factors (surface erosion/deposition and constant sedimentation rate) to homogenous lithospheres and accretionary lithospheres (Archean and Proterozoic). From the analysis of the simulations, we can state that:

The presence of a thermal anomaly alone is not sufficient to create long-lived basins. Even with erosion sedimentation processes, thermal subsidence is largely reduced after 50 Myr and completely ceased after 150 Myr.

Arches and Basins can emerge from the amplification of the geometry of the terranes through differential erosion sedimentation of Archean/Proterozoic terranes (columns) with different rheologies/densities.

The sedimentation rates control the duration of subsidence, typically over 250 Myr in intra-continental context where there are no mountain ranges to provide large sediment supply.

Local sediment supply alone can't cover the arches while remote sediment supply is necessary to both increase the thickness of basin and rise the temperature (supported by the slow burial of radiogenic heat from the basement).

Far field stresses lead to more asymmetric basins and result in the formation intra-basins arches and inter-basin boundary secondary arches delimited by fault-related sub-basins (grabens). They can explain dissimilarities of sedimentary fillings between neighbouring basins as well as the presence of unconformities in the deeper part of the basins.

The effects of tectonics are amplified when a deep-seated thermal anomaly weakens the lithosphere.

The sedimentary piles record complex hiatus, truncation and onlap terminations that differ between the various basins even if the boundary conditions in term of far field stresses are the same. Such a complexity has been often noticed by many geologists when trying to do well correlations in the Saharan Platform (*e.g.* Perron *et al.*, 2018), for instance.

Erosion/deposition alone cannot dissipate the isostatic potential (gravitational potential energy) because of the strength of the lithosphere (regional isostasy) resists to complete re-equilibration. However, far field stresses or/and thermal events can temporally drop the lithospheric strength and allow subsidence driven by isostatic potential.

Taken as keys to interpret real dataset, we believe that the simulations presented here are simple but realistic enough to constitute a step forward in tectono-stratigraphic trap prediction and heat flux analysis in intracratonic basins.

Supplementary Material

Suppl. 1. Isostasy.
Suppl. 2. Model M: Heterogeneous lithosphere alternation archean/proterozoic terranes.
Suppl. 3. Subisdence curves of wells.
Suppl. 4. Model M: Heterogeneous lithosphere alternation archean/proterozoic terranes.

The Supplementary Material is available at http://www.bsgf.fr/10.1051/bsgf/2020038/olm.

Data availability statement

The data that support the findings of this study are available from the corresponding author upon reasonable request.

Acknowledgements. We are most grateful to Neptune energy and ENGIE who funded this work and provided the geological database (seismic profiles and wells) of Algeria used in this paper. Special thanks to Anthony Jourdon for his help on Matlab scripts. Thanks also go to Sierd Cloetingh, Rémi Eschard and anonymous reviewers who have enriched and considerably improved this paper.

References

Adkinson W. 1966. Stratigraphic cross section of Paleozoic rocks, Colorado to New York. Cross-section Publication 4. American Association of Petroleum Geologists, 58 p.

Akkouche MM. 2007. Application de la datation par traces de fission à l'analyse de la thermicité de bassins à potentialités pétrolières. Exemple de la cuvette de Sbaâ et du bassin de l'Ahnet-Nord (plateforme saharienne occidentale, Algérie). Université Bordeaux 1.

Allen PA, Allen JR. 2013. Basin analysis: principles and application to petroleum play assessment, 3rd ed. Chichester, West Susex, UK: Wiley-Blackwell.

Allen PA, Armitage JJ. 2011. Cratonic Basins. In: Busby C, Azor A, eds. *Tectonics of Sedimentary Basins*. John Wiley & Sons Ltd., pp. 602–620.

Armitage JJ, Allen PA. 2010. Cratonic basins and the long-term subsidence history of continental interiors. *J. Geol. Soc.* 167(1): 61–70. https://doi.org/10.1144/0016-76492009-108.

Artemieva IM. 2009. The continental lithosphere: Reconciling thermal, seismic, and petrologic data. *Lithos* 109(1-2): 23–46. https://doi.org/10.1016/j.lithos.2008.09.015.

Artemieva IM, Mooney WD. 2002. On the relations between cratonic lithosphere thickness, plate motions, and basal drag. *Tectonophysics* 358(1-4): 21. https://doi.org/10.1016/S0040-1951(02)00425-0.

Audet P, Bürgmann R. 2011. Dominant role of tectonic inheritance in supercontinent cycles. *Nat. Geosci.* 4(3): 184–187. https://doi.org/10.1038/ngeo1080.

Avigad D, Gvirtzman Z. 2009. Late Neoproterozoic rise and fall of the northern Arabian–Nubian shield: The role of lithospheric mantle delamination and subsequent thermal subsidence. *Tectonophysics* 477(3): 217–228. https://doi.org/10.1016/j.tecto.2009.04.018.

Avouac JP, Burov EB. 1996. Erosion as a driving mechanism of intracontinental mountain growth. *J. Geophys. Res. Solid Earth* 101 (B8): 17747–17769. https://doi.org/10.1029/96JB01344.

Baird DJ, Knapp JH, Steer DN, Brown LD, Nelson KD. 1995. Upper-mantle reflectivity beneath the Williston basin, phase-change Moho, and the origin of intracratonic basins. *Geology* 23(5): 431–434.

Balay S, Abhyankar S, Adams M, Brown J, Brune P, Buschelman K, *et al.* 2017. PETSc Users Manual Revision 3.8. Argonne, IL (United States): Argonne National Lab (ANL).

Beaumont C, Fullsack P, Hamilton J. 1992. Erosional control of active compressional orogens. In: *Thrust tectonics*. Springer, pp. 1–18.

Bertrand JML, Caby R. 1978. Geodynamic evolution of the Pan-African orogenic belt: A new interpretation of the Hoggar shield (Algerian Sahara). *Geol. Rundsch.* 67(2): 357–388. https://doi.org/10.1007/BF01802795.

Beuf S, Biju-Duval B, De Charpal O, Gariel O, Bennacef A, Black R, *et al*. 1968. Une conséquence directe de la structure du bouclier Africain : l'ébauche des bassins de l'Ahnet et du Mouydir au Paléozoique inférieur. *Publ. Serv. Géologique L'Algérie Nouv. Sér. Bull.* 38: 105–34.

Beuf S, Biju-Duval B, de Charpal O, Rognon P, Gabriel O, Bennacef A. 1971. Les grès du Paléozoïque inférieur au Sahara : sédimentation et discontinuités évolution structurale d'un craton. Paris : Technip.

Black R, Latouche L, Liégeois JP, Caby R, Bertrand JM. 1994. Pan-African displaced terranes in the Tuareg shield (central Sahara). *Geology* 22(7): 641–644.

Bologna MS, Nunes HO, Padilha AL, Vitorello Í, Pádua MB. 2013. Anomalous electrical structure in the northwestern Paraná Basin, Brazil, observed with broadband magnetotellurics. *J. South Am. Earth Sci.* 42: 74–82. https://doi.org/10.1016/j.jsames.2012.07.006.

Bond GC, Kominz MA. 1991. Disentangling middle Paleozoic sea level and tectonic events in cratonic margins and cratonic basins of North America. *J. Geophys. Res. Solid Earth* 96(B4): 6619–6639.

Boote DRD, Clark-Lowes DD, Traut MW. 1998. Palaeozoic petroleum systems of North Africa. *Geol. Soc. Lond. Spec. Publ.* 132(1): 7–68. https://doi.org/10.1144/GSL.SP.1998.132.01.02.

Bouzid A, Akacem N, Hamoudi M, Ouzegane K, Abtout A, Kienast J-R. 2008. Modélisation magnétotellurique de la structure géologique profonde de l'unité granulitique de l'In Ouzzal (Hoggar occidental). *Comptes Rendus Geosci.* 340(11): 711–722. https://doi.org/10.1016/j.crte.2008.08.001.

Brace WF, Kohlstedt DL. 1980. Limits on lithospheric stress imposed by laboratory experiments. *J. Geophys. Res. Solid Earth* 85(B11): 6248–6252. https://doi.org/10.1029/JB085iB11p06248.

Brahimi S, Liégeois J-P, Ghienne J-F, Munschy M, Bourmatte A. 2018. The Tuareg shield terranes revisited and extended towards the northern Gondwana margin: Magnetic and gravimetric constraints. *Earth-Sci. Rev.*

Brunet M-F, Pichon XL. 1982. Subsidence of the Paris Basin. *J. Geophys. Res. Solid Earth* 87(B10): 8547–8560. https://doi.org/10.1029/JB087iB10p08547.

Buiter SJH, Pfiffner OA. 2003. Numerical models of the inversion of half-graben basins. *Tectonics* 22(5). https://doi.org/10.1029/2002TC001417.

Burov EB, Diament M. 1995. The effective elastic thickness (Te) of continental lithosphere: what does it really mean? *J. Geophys. Res. Solid Earth* 100(B3): 3905–3927.

Burov E, Poliakov A. 2001. Erosion and rheology controls on synrift and postrift evolution: Verifying old and new ideas using a fully coupled numerical model. *J. Geophys. Res. Solid Earth* 106(B8): 16461–16481.

Cacace M, Scheck-Wenderoth M. 2016. Why intracontinental basins subside longer: 3-D feedback effects of lithospheric cooling and sedimentation on the flexural strength of the lithosphere: Subsidence at Intracontinental Basins. *J. Geophys. Res. Solid Earth* 121(5): 3742–3761. https://doi.org/10.1002/2015JB012682.

Cagnard F, Barbey P, Gapais D. 2011. Transition between "Archaean-type" and "modern-type" tectonics: Insights from the Finnish Lapland Granulite Belt. *Precambrian Res.* 187(1-2): 127–142. https://doi.org/10.1016/j.precamres.2011.02.007.

Caravaca G, Brayard A, Vennin E, Guiraud M, Le Pourhiet L, Grosjean A-S, *et al.* 2017. Controlling factors for differential subsidence in the Sonoma Foreland Basin (Early Triassic, western USA). *Geol. Mag.* 1–25. https://doi.org/10.1017/S0016756817000164.

Carter NL, Tsenn MC. 1987. Flow properties of continental lithosphere. *Tectonophysics* 136(1-2): 27–63.

Cawood PA, ed. 2009. *Earth accretionary systems in space and time*. Geological Soc London.

Cawood PA, Kröner A, Collins WJ, Kusky TM, Mooney WD, Windley BF. 2009. Accretionary orogens through Earth history. *Geol. Soc. Lond. Spec. Publ.* 318(1): 1–36. https://doi.org/10.1144/SP318.1.

Célérier J, Sandiford M, Hansen DL, Quigley M. 2005. Modes of active intraplate deformation, Flinders Ranges, Australia. *Tectonics* 24(6): 1–17. https://doi.org/10.1029/2004TC001679.

Chardon D, Gapais D, Cagnard F. 2009. Flow of ultra-hot orogens: A view from the Precambrian, clues for the Phanerozoic. *Tectonophysics* 477(3-4): 105–118. https://doi.org/10.1016/j.tecto.2009.03.008.

Cherepanova Y, Artemieva IM. 2015. Density heterogeneity of the cratonic lithosphere: A case study of the Siberian Craton. *Gondwana Res.* 28(4): 1344–1360. https://doi.org/10.1016/j.gr.2014.10.002.

Cherepanova Y, Artemieva IM, Thybo H, Chemia Z. 2013. Crustal structure of the Siberian craton and the West Siberian basin: An appraisal of existing seismic data. *Tectonophysics* 609: 154–183. https://doi.org/10.1016/j.tecto.2013.05.004.

Chernicoff CJ, Zappettini EO. 2004. Geophysical Evidence for Terrane Boundaries in South-Central Argentina. *Gondwana Res.* 7 (4): 1105–1116. https://doi.org/10.1016/S1342-937X(05)71087-X.

Cloetingh S. 1986. Intraplate stresses: A new tectonic mechanism for fluctuations of relative sea level. *Geology* 14(7): 617–620. https://doi.org/10.1130/0091-7613(1986)14<617:ISANTM>2.0.CO;2.

Cloetingh S. 1988. Intraplate stresses: A new element in basin analysis. In: K. L. Kleinspehn and C. Paola, eds. *New Perspectives in Basin Analysis*. New York, NY.: Springer New York, pp. 205–230.

Cloetingh S, Burov E. 2011. Lithospheric folding and sedimentary basin evolution: a review and analysis of formation mechanisms. *Basin Res.* 23(3): 257–290. https://doi.org/10.1111/j.1365-2117.2010.00490.x.

Cloetingh S, McQueen H, Lambeck K. 1985. On a tectonic mechanism for regional sealevel variations. *Earth Planet. Sci. Lett.* 75(2): 157–166. https://doi.org/10.1016/0012-821X(85)90098-6.

Condie KC. 2007. Accretionary orogens in space and time. In: *Geological Society of America Memoirs*, vol. 200, pp. 145–158. Geological Society of America.

Conrad J. 1984. Les séries carbonifères du Sahara central algérien: stratigraphie, sédimentation, évolution structurale. Doctoral dissertation, Université Aix-Marseille III, France.

Coward MP, Ries AC. 2003. Tectonic development of North African basins. *Geol. Soc. Lond. Spec. Publ.* 207(1): 61–83. https://doi.org/10.1144/GSL.SP.2003.207.4.

Craig J, Rizzi C, Said F, Thusu B, Luning S, Asbali AI, *et al.* 2008. Structural styles and prospectivity in the Precambrian and Palaeozoic hydrocarbon systems of North Africa. *Geol. East Libya* 4: 51–122.

Culling WEH. 1965. Theory of erosion on soil-covered slopes. *J. Geol.* 73(2): 230–254.

Daly MC, Andrade V, Barousse CA, Costa R, McDowell K, Piggott N, *et al.* 2014. Brasiliano crustal structure and the tectonic setting of the Parnaíba basin of NE Brazil: Results of a deep seismic reflection profile. *Tectonics* 33(11): 2102–2120. https://doi.org/10.1002/2014TC003632.

Daly MC, Tozer B, Watts AB. 2018. Cratonic basins and the Wilson cycle: a perspective from the Parnaíba Basin, Brazil. *Geol. Soc. Lond. Spec. Publ.* 470: SP470.13. https://doi.org/10.1144/SP470.13.

de Brito Neves BB, Fuck RA, Cordani UG, Thomaz FA. 1984. Influence of basement structures on the evolution of the major sedimentary basins of Brazil: A case of tectonic heritage. *J. Geodyn.* 1(3): 495–510. https://doi.org/10.1016/0264-3707(84)90021-8.

de Wit MJ, Linol B. 2015. Precambrian basement of the Congo Basin and its flanking terrains. In: *Geology and Resource Potential of the Congo Basin*. Springer, pp. 19–37.

de Wit MJ, de Ronde CEJ, Tredoux M, Roering C, Hart RJ, Armstrong RA, *et al.* 1992. Formation of an Archaean continent. *Nature* 357(6379): 553–562. https://doi.org/10.1038/357553a0.

Derder MEM, Maouche S, Liégeois JP, Henry B, Amenna M, Ouabadi A, *et al.* 2016. Discovery of a Devonian mafic magmatism on the western border of the Murzuq basin (Saharan metacraton): Paleomagnetic dating and geodynamical implications. *J. Afr. Earth Sci.* 115: 159–176. https://doi.org/10.1016/j.jafrearsci.2015.11.019.

DeRito RF, Cozzarelli FA, Hodge DS. 1983. Mechanism of subsidence of ancient cratonic rift basins. *Tectonophysics* 94(1): 141–168. https://doi.org/10.1016/0040-1951(83)90014-8.

Djomani YHP, O'Reilly SY, Griffin WL, Morgan P. 2001. The density structure of subcontinental lithosphere through time. *Earth Planet. Sci. Lett.* 184(3-4): 605–621. https://doi.org/10.1016/S0012-821X(00)00362-9.

Eschard R, Braik F, Bekkouche D, Rahuma MB, Desaubliaux G, Deschamps R, Proust JN. 2010. Palaeohighs: their influence on the North African Palaeozoic petroleum systems. *Pet. Geol. Mature Basins New Front.* In: *7th Pet. Geol. Conf.*, pp. 707–724.

Eaton DW, Darbyshire F. 2010. Lithospheric architecture and tectonic evolution of the Hudson Bay Region. *Tectonophysics* 480(1-4): 1–22. https://doi.org/10.1016/j.tecto.2009.09.006.

Fishwick S, Bastow ID. 2011. Towards a better understanding of African topography: a review of passive-source seismic studies of the African crust and upper mantle. *Geol. Soc. Lond. Spec. Publ.* 357(1): 343–371. https://doi.org/10.1144/SP357.19.

Fowler CMR, Nisbet EG. 1985. The subsidence of the Williston Basin. *Can. J. Earth Sci.* 22(3): 408–415. https://doi.org/10.1139/e85-039.

Frederiksen AW, Deniset I, Ola O, Toni D. 2013. Lithospheric fabric variations in central North America: Influence of rifting and Archean tectonic styles. *Geophys. Res. Lett.* 40(17): 4583–4587.

Gac S, Huismans RS, Simon NSC, Podladchikov YY, Faleide JI. 2013. Formation of intracratonic basins by lithospheric shortening and phase changes: a case study from the ultra-deep East Barents Sea Basin. *Terra Nova* 25(6): 459–464. https://doi.org/10.1111/ter.12057.

Gleason GC, Tullis J. 1995. A flow law for dislocation creep of quartz aggregates determined with the molten salt cell. *Tectonophysics* 247(1-4): 1–23.

Goetze C, Evans B. 1979. Stress and temperature in the bending lithosphere as constrained by experimental rock mechanics. *Geophys. J. R. Astron. Soc.* 59(3): 463–478. https://doi.org/10.1111/j.1365-246X.1979.tb02567.x.

Guiraud R, Bosworth W, Thierry J, Delplanque A. 2005. Phanerozoic geological evolution of Northern and Central Africa: An overview. *J. Afr. Earth Sci.* 43(1-3): 83–143. https://doi.org/10.1016/j.jafrearsci.2005.07.017.

Gwavava O, Swain CJ, Podmore F. 1996. Mechanisms of isostatic compensation of the Zimbabwe and Kaapvaal cratons, the Limpopo Belt and the Mozambique basin. *Geophys. J. Int.* 127 (3), 635–650.

Haddoum H, Guiraud R, Moussine-Pouchkine A. 2001. Hercynian compressional deformations of the Ahnet–Mouydir Basin, Algerian Saharan Platform: far-field stress effects of the Late Palaeozoic orogeny. *Terra Nova* 13(3): 220–226.

Hamdani Y, Mareschal J-C, Arkani-Hamed J. 1991. Phase changes and thermal subsidence in intracontinental sedimentary basins. *Geophys. J. Int.* 106(3): 657–665. https://doi.org/10.1111/j.1365-246X.1991.tb06337.x.

Hartley RW, Allen PA. 1994. Interior cratonic basins of Africa: relation to continental break-up and role of mantle convection. *Basin Res.* 6(2-3): 95–113.

Hartley R, Watts AB, Fairhead JD. 1996. Isostasy of Africa. *Earth Planet. Sci. Lett.* 137(1): 1–18. https://doi.org/10.1016/0012-821X(95)00185-F.

Haxby WF, Turcotte DL, Bird JM. 1976. Thermal and Mechanical Evolution of the Michigan Basin. *Dev. Geotecton.* 12: 57–75. https://doi.org/10.1016/B978-0-444-41549-3.50008-6.

Heilbron M, Valeriano CM, Tassinari CCG, Almeida J, Tupinambá M, Siga O, *et al.* 2008. Correlation of Neoproterozoic terranes

between the Ribeira Belt, SE Brazil and its African counterpart: comparative tectonic evolution and open questions. *Geol. Soc. Lond. Spec. Publ.* 294(1): 211–237.

Heine C, Dietmar Müller R, Steinberger B, Torsvik TH. 2008. Subsidence in intracontinental basins due to dynamic topography. *Phys. Earth Planet. Inter.* 171(1-4): 252–264. https://doi.org/10.1016/j.pepi.2008.05.008.

Heron PJ, Pysklywec RN, Stephenson R. 2016. Lasting mantle scars lead to perennial plate tectonics. *Nat. Commun.* 7(1): 11834. https://doi.org/10.1038/ncomms11834.

Holt P. 2012. Subsidence Mechanisms of Sedimentary Basins Developed over Accretionary Crust. Doctoral, Durham University. Available at http://etheses.dur.ac.uk/3584/ (Accessed 22 November 2016).

Holt PJ, Allen MB, van Hunen J, Bjørnseth HM. 2010. Lithospheric cooling and thickening as a basin forming mechanism. *Tectonophysics* 495(3-4): 184–194. https://doi.org/10.1016/j.tecto.2010.09.014.

Holt PJ, Allen MB, van Hunen J. 2015. Basin formation by thermal subsidence of accretionary orogens. *Tectonophysics* 639: 132–143. https://doi.org/10.1016/j.tecto.2014.11.021.

Howell PD, van der Pluijm BA. 1990. Early history of the Michigan basin: Subsidence and Appalachian tectonics. *Geology* 18(12): 1195–1198. https://doi.org/10.1130/0091-7613(1990)018<1195:EHOTMB>2.3.CO;2.

Howell PD, van der Pluijm BA. 1999. Structural sequences and styles of subsidence in the Michigan basin. *Geol. Soc. Am. Bull.* 111(7): 974–991. https://doi.org/10.1130/0016-7606(1999)111<0974:SSASOS>2.3.CO;2.

Huismans RS, Beaumont C. 2002. Asymmetric lithospheric extension: The role of frictional plastic strain softening inferred from numerical experiments. *Geology* 30(3): 211–214.

Janssen ME, Stephenson RA, Cloetingh S. 1995. Temporal and spatial correlations between changes in plate motions and the evolution of rifted basins in Africa. *Geol. Soc. Am. Bull.* 107(11), 1317–1332.

Jourdon A, Le Pourhiet L, Petit C, Rolland Y. 2017. The deep structure and reactivation of the Kyrgyz Tien Shan: Modelling the past to better constrain the present. *Tectonophysics*. https://doi.org/10.1016/j.tecto.2017.07.019.

Jourdon A, Le Pourhiet L, Petit C, Rolland Y. 2018. Impact of range-parallel sediment transport on 2D thermo-mechanical models of mountain belts: Application to the Kyrgyz Tien Shan. *Terra Nova* 30(4): 279–288. https://doi.org/10.1111/ter.12337.

Kaus B, Connolly J, Podladchikov Y, Schmalholz S. 2005. Effect of mineral phase transitions on sedimentary basin subsidence and uplift. *Earth Planet. Sci. Lett.* 233(1-2): 213–228. https://doi.org/10.1016/j.epsl.2005.01.032.

Klein G. deV, Hsui AT. 1987. Origin of cratonic basins. *Geology* 15 (12): 1094–1098. https://doi.org/10.1130/0091-7613(1987)15<1094:OOCB>2.0.CO;2.

Kracha N. 2011. Relation entre sédimentologie, fracturation naturelle et diagénèse d'un réservoir à faible perméabilité application aux réservoirs de l'Ordovicien bassin de l'Ahnet, Sahara central, Algérie. Doctoral dissertation, Université des sciences et technologies de Lille, France.

Kreemer C, Blewitt G, Klein EC. 2014. A geodetic plate motion and Global Strain Rate Model. *Geochem. Geophys. Geosystems* 15(10): 3849–3889. https://doi.org/10.1002/2014GC005407.

Lafosse M, Boutoux A, Bellahsen N, Le Pourhiet L. 2016. Role of tectonic burial and temperature on the inversion of inherited extensional basins during collision. *Geol. Mag.* 153(5-6): 811–826. https://doi.org/10.1017/S0016756816000510.

Lambeck K. 1983. The role of compressive forces in intracratonic basin formation and mid-plate orogenies. *Geophys. Res. Lett.* 10 (9): 845–848. https://doi.org/10.1029/GL010i009p00845.

Le Pourhiet L, Burov E, Moretti I. 2004. Rifting through a stack of inhomogeneous thrusts (the dipping pie concept). *Tectonics* 23(4). https://doi.org/10.1029/2003TC001584.

Lessard L. 1961. Les series primaires des Tassilis Oua-n-Ahaggar au sud du Hoggar entre l'Ar et l'Adrar des Iforas (Sahara meridional). *Bull. Société Géologique Fr.* S7-III(5): 501–513. https://doi.org/10.2113/gssgfbull.S7-III.5.501.

Liégeois J-P. 2019. A new synthetic geological map of the tuareg shield: An overview of its global structure and geological evolution. In: A. Bendaoud, Z. Hamimi, M. Hamoudi, S. Djemai, B. Zoheir, eds. *The Geology of the Arab World – An Overview*. Cham: Springer International Publishing, pp. 83–107.

Liégeois JP, Sauvage JF, Black R. 1991. The Permo-Jurassic alkaline province of Tadhak, Mali: Geology, geochronology and tectonic significance. *Lithos* 27(2): 95–105. https://doi.org/10.1016/0024-4937(91)90022-D,

Liégeois J-P, Benhallou A, Azzouni-Sekkal A, Yahiaoui R, Bonin B. 2005. The Hoggar swell and volcanism: Reactivation of the Precambrian Tuareg shield during Alpine convergence and West African Cenozoic volcanism. *Geol. Soc. Am. Spec. Pap.* 388: 379–400. https://doi.org/10.1130/0-8137-2388-4.379.

Logan P, Duddy I. 1998. An investigation of the thermal history of the Ahnet and Reggane Basins, Central Algeria, and the consequences for hydrocarbon generation and accumulation. *Geol. Soc. Lond. Spec. Publ.* 132(1): 131–155.

Lüning S, Craig J, Loydell DK, Štorch P, Fitches B. 2000. Lower Silurian "hot shales" in North Africa and Arabia: regional distribution and depositional model. *Earth-Sci. Rev.* 49(1-4): 121–200. https://doi.org/10.1016/S0012-8252(99)00060-4.

Lüning S, Adamson K, Craig J. 2003. Frasnian organic-rich shales in North Africa: regional distribution and depositional model. *Geol. Soc. Lond. Spec. Publ.* 207(1): 165–184. https://doi.org/10.1144/GSL.SP.2003.207.9.

Lyatsky H, Friedman GM, Lyatsky VB. 2006. Principles of practical tectonic analysis of cratonic regions: With particular reference to Western North America. Springer.

Mackwell SJ, Zimmerman ME, Kohlstedt DL. 1998. High-temperature deformation of dry diabase with application to tectonics on Venus. *J. Geophys. Res. Solid Earth* 103(B1), 975–984.

Mantovani MSM, Quintas MCL, Shukowsky W, Brito Neves BB. 2005. Delimitation of the Paranapanema Proterozoic block: a geophysical contribution. *Episodes-Newsmag. Int. Union Geol. Sci.* 28(1): 18–22.

May DA, Brown J, Pourhiet LL. 2014. pTatin3D: High-performance methods for long-term lithospheric dynamics. In: *SC '14: Proceedings of the International Conference for High Performance Computing, Networking, Storage and Analysis*, pp. 274–284.

May DA, Brown J, Le Pourhiet L. 2015. A scalable, matrix-free multigrid preconditioner for finite element discretizations of heterogeneous Stokes flow. *Comput. Methods Appl. Mech. Eng.* 290: 496–523. https://doi.org/10.1016/j.cma.2015.03.014.

McKenzie D. 1978. Some remarks on the development of sedimentary basins. *Earth Planet. Sci. Lett.* 40(1): 25–32. https://doi.org/10.1016/0012-821X(78)90071-7.

McKenzie D, Priestley K. 2016. Speculations on the formation of cratons and cratonic basins. *Earth Planet. Sci. Lett.* 435: 94–104. https://doi.org/10.1016/j.epsl.2015.12.010.

Moreau C, Demaiffe D, Bellion Y, Boullier A-M. 1994. A tectonic model for the location of Palaeozoic ring complexes in Air (Niger, West Africa). *Tectonophysics* 234(1): 129–146.

Moretti I, Froidevaux C. 1986. Thermomechanical models of active rifting. *Tectonics* 5(4): 501–511.

Moretti I, Turcotte DL. 1985. A model for erosion, sedimentation, and flexure with application to New Caledonia. *J. Geodyn.* 3(1): 155–168. https://doi.org/10.1016/0264-3707(85)90026-2.

Naimark BM, Ismail-Zadeh AT. 1995. Numerical models of a subsidence mechanism in intracratonic basins: application to North American basins. *Geophys. J. Int.* 123(1): 149–160. https://doi.org/10.1111/j.1365-246X.1995.tb06667.x.

Nikishin AM, Ziegler PA, Abbott D, Brunet M-F, Cloetingh S. 2002. Permo–Triassic intraplate magmatism and rifting in Eurasia: implications for mantle plumes and mantle dynamics. *Tectonophysics* 351(1-2): 3–39.

Nunn JA. 1994. Free thermal convection beneath intracratonic basins: thermal and subsidence effects. *Basin Res.* 6(2-3): 115–130.

Nunn JA, Sleep NH. 1984. Thermal contraction and flexure of intracratonal basins: a three-dimensional study of the Michigan basin. *Geophys. J. Int.* 76(3): 587–635. https://doi.org/10.1111/j.1365-246X.1984.tb01912.x.

Nunn JA, Sleep NH, Moore WE. 1984. Thermal Subsidence and Generation of Hydrocarbons in Michigan Basin. *AAPG Bull.* 68. https://doi.org/10.1306/AD460A17-16F7-11D7-8645000102C1865D.

Parsons B, Sclater JG. 1977. An analysis of the variation of ocean floor bathymetry and heat flow with age. *J. Geophys. Res.* 82(5): 803–827.

Peace A, McCaffrey K, Imber J, van Hunen J, Hobbs R, Wilson R. 2018. The role of pre-existing structures during rifting, continental breakup and transform system development, offshore West Greenland. *Basin Res.* 30(3), 373–394.

Perron P. 2019. Architecture and tectonic of Paleozoic intracratonic Basins: Impact on the sedimentary record and associated geometries. Example of peri-Hoggar Basins (North Gondwana marge). Dijon: Université de Bourgogne Franche-Comté.

Perron P, Guiraud M, Vennin E, Moretti I, Portier É, Le Pourhiet L, *et al.* 2018. Influence of basement heterogeneity on the architecture of low subsidence rate Paleozoic intracratonic basins (Reggane, Ahnet, Mouydir and Illizi basins, Hoggar Massif). *Solid Earth* 9(6): 1239–1275. https://doi.org/10.5194/se-9-1239-2018.

Phillips TB, Jackson CA-L, Bell RE, Duffy OB. 2018. Oblique reactivation of lithosphere-scale lineaments controls rift physiography – The upper-crustal expression of the Sorgenfrei-Tornquist Zone, offshore southern Norway. *Solid Earth* 9(2): 403–429. https://doi.org/10.5194/se-9-403-2018.

Quinlan G. 1987. Models of subsidence mechanisms in intracratonic basins, and their applicability to North American examples. pp. 463–481.

Ranalli G. 2000. Rheology of the crust and its role in tectonic reactivation. *J. Geodyn.* 30(1-2): 3–15. https://doi.org/10.1016/S0264-3707(99)00024-1.

Ratheesh-Kumar RT, Windley BF, Sajeev K. 2014. Tectonic inheritance of the Indian Shield: New insights from its elastic thickness structure. *Tectonophysics* 615-616: 40–52. https://doi.org/10.1016/j.tecto.2013.12.010.

Rougier S, Missenard Y, Gautheron C, Barbarand J, Zeyen H, Pinna R, *et al.* 2013. Eocene exhumation of the Tuareg Shield (Sahara Desert, Africa). *Geology* 41(5): 615–618. https://doi.org/10.1130/G33731.1.

Rybacki E, Dresen G. 2000. Dislocation and diffusion creep of synthetic anorthite aggregates. *J. Geophys. Res. Solid Earth* 105 (B11): 26017–26036.

Sandiford M, McLaren S. 2002. Tectonic feedback and the ordering of heat producing elements within the continental lithosphere. *Earth Planet. Sci. Lett.* 204(1-2): 133–150.

Scheck M, Bayer U. 1999. Evolution of the Northeast German Basin – Inferences from a 3D structural model and subsidence analysis. *Tectonophysics* 313(1): 145–169. https://doi.org/10.1016/S0040-1951(99)00194-8.

Seyfert CK. 1987. Cratonic basins, domes, and arches. In: *Structural Geology and Tectonics*. Berlin, Heidelberg: Springer Berlin Heidelberg, pp. 141–158.

Sleep NH, Sloss LL. 1978. A deep borehole in the Michigan Basin. *J. Geophys. Res. Solid Earth* 83(B12): 5815–5819. https://doi.org/10.1029/JB083iB12p05815.

Sleep NH, Nunn JA, Chou L. 1980. Platform basins. *Annu. Rev. Earth Planet. Sci.* 8: 17.

Smith R. 1967. Stratigraphic cross-section of Paleozoic rocks, Oklahoma to Saskatchewan. Cross-section Publication 5. American Association of Petroleum Geologists.

Tesauro M, Audet P, Kaban MK, Bürgmann R, Cloetingh S. 2012. The effective elastic thickness of the continental lithosphere: Comparison between rheological and inverse approaches: *Te* of the continental lithosphere. *Geochem. Geophys. Geosystems* 13(9). https://doi.org/10.1029/2012GC004162.

Tesauro M, Kaban MK, Mooney WD. 2015. Variations of the lithospheric strength and elastic thickness in North America: Lithosphere strenght and TE variations. *Geochem. Geophys. Geosystems* 16(7): 2197–2220. https://doi.org/10.1002/2015GC005937.

Tozer B, Watts AB, Daly MC. 2017. Crustal structure, gravity anomalies, and subsidence history of the Parnaíba cratonic basin, Northeast Brazil. *J. Geophys. Res. Solid Earth* 122(7): 5591–5621. https://doi.org/10.1002/2017JB014348.

Turcotte DL, Schubert G. 2014. Geodynamics, 3rd ed. Cambridge, United Kingdom: Cambridge University Press.

von Tscharner M, Schmalholz SM, Epard J-L. 2016. 3-D numerical models of viscous flow applied to fold nappes and the Rawil depression in the Helvetic nappe system (western Switzerland). *J. Struct. Geol.* 86: 32–46. https://doi.org/10.1016/j.jsg.2016.02.007.

Watremez L, Burov E, d'Acremont E, Leroy S, Huet B, Le Pourhiet L, Bellahsen N. 2013. Buoyancy and localizing properties of continental mantle lithosphere: Insights from thermomechanical models of the eastern Gulf of Aden. *Geochemistry, Geophysics, Geosystems* 14(8): 2800–2817.

Wells M, Hirst P, Bouch J, Whear E, Clark N. 2018. Deciphering multiple controls on reservoir quality and inhibition of quartz cement in a complex reservoir: Ordovician glacial sandstones, Illizi Basin, Algeria. *Geol. Soc. Lond. Spec. Publ.* 435(1): 343–372. https://doi.org/10.1144/SP435.6.

Wendt J, Kaufmann B, Belka Z, Klug C, Lubeseder S. 2006. Sedimentary evolution of a Palaeozoic basin and ridge system: the Middle and Upper Devonian of the Ahnet and Mouydir (Algerian Sahara). *Geol. Mag.* 143(3): 269–299. https://doi.org/10.1017/S0016756806001737.

Wendt J, Kaufmann B, Belka Z, Korn D. 2009. Carboniferous stratigraphy and depositional environments in the Ahnet Mouydir area (Algerian Sahara). *Facies* 55(3): 443–472. https://doi.org/10.1007/s10347-008-0176-y.

Xie X, Heller P. 2009. Plate tectonics and basin subsidence history. *Geol. Soc. Am. Bull.* 121(1-2): 55–64. https://doi.org/10.1130/B26398.1.

Yahi N. 1999. Petroleum generation and migration in the Berkine (Ghadames) Basin, Eastern Algeria: an organic geochemical and basin modelling study. Doctoral dissertation, Forschungszentrum, Zentralbibliothek, Jülich.

Zazoun RS. 2001. Hercynian deformation in the western Ahnet Basin and Bled El-Mass area, Algerian Sahara: a continuous strain. *J. Afr. Earth Sci.* 32(4): 869–887.

Ziegler PA, Cloetingh S, van Wees J-D. 1995. Dynamics of intra-plate compressional deformation: the Alpine foreland and other examples. *Tectonophysics* 252(1): 7–59. https://doi.org/10.1016/0040-1951(95)00102-6.

Zieliński M. 2012. Conodont thermal alteration patterns in Devonian and Carboniferous rocks of the Ahnet and Mouydir basins (southern Algeria). *Mar. Pet. Geol.* 38(1): 166–176.

Appendix A Numerical method

In order to study the influence of accreted lithospheric heterogeneities on the architecture and the low long-lived subsidence of intracratonic basins, we use the thermo-mechanical numerical code pTatin (May *et al.*, 2014, 2015) in its 2D version (Jourdon *et al.*, 2017). The code relies on PETSc library Balay *et al.* (2017) to solve conservation of momentum

$$\nabla.\sigma = \rho g,$$

for an incompressible fluid flow described by its velocity v such as

$$\nabla.\mathbf{v} = 0,$$

using high order Q2P1 finite elements in parallel. This permits to model accurately the topography with a free surface. In order to avoid deformation of the mesh the lithologies are tracked with ALE marker in cell approach (May *et al.*, 2015). Markers are used to carry lithological properties. The density ρ_0 is one of them, but effective density ρ also depends on temperature T and pressure P using Boussinesq approximation, where α and β are the coefficient of thermal expansion and adiabatic compressibility respectively.

$$\rho = (1 - \alpha\Delta T + \beta P)\rho 0.$$

Stress ($\boldsymbol{\sigma}$) and strain rate ($\dot{\varepsilon}$) are also computed on markers in two stages. In a first trial, the code evaluates the stress considering the fluid/rocks deform by dislocation creep

$$\sigma = A^{\frac{-1}{n}} \exp^{\frac{Q}{nRT}} \dot{\varepsilon}^{II\frac{1-n}{n}} \dot{\varepsilon},$$

and therefore, its effective viscosity depends on temperature T, lithology (A, n, Q see Tab. 1) and the second invariant of strain rate ($\dot{\varepsilon}^{II}$). However, when this trial viscous stress exceeds brittle frictional brittle strength $\sigma^b = \sin\varphi + C\cos\varphi$ or maximum plastic strength σ^p fixed at 450 MPa (stress/viscosity limiter; Watremez *et al.*, 2013), the effective viscosity is adjusted to

$$\eta = \frac{\sigma^\gamma}{2\dot{\varepsilon}^{II}},$$

in order to keep the stress on the yield cap defined as $\sigma^\gamma = \min(\sigma^b, \sigma^p)$.

Conservation of momentum is coupled with conservation of heat

$$\frac{\partial T}{\partial t} = \nabla.\kappa\nabla T + \mathrm{v}\nabla T + \frac{H}{Cp}.$$

.

The heat diffusivity k, heat production H and heat capacity Cp do not vary for the different simulations.

Sediment transport is simulated using advection diffusion of the topography in 1D

$$\frac{\partial h}{\partial t} = \mathrm{v}_y + \frac{\partial}{\partial x}\left(ke\frac{\partial h}{\partial x}\right) + \mathrm{S},$$

with a source term S, which permits out-of-plane sediments inflow and outflow. Details about the implementation and tracking of the stratigraphy may be found in Jourdon *et al.* (2018).

Cite this article as: Perron P, Le Pourhiet L, Guiraud M, Vennin E, Moretti I, Portier É, Konaté M. 2021. Control of inherited accreted lithospheric heterogeneity on the architecture and the low, long-term subsidence rate of intracratonic basins, *BSGF - Earth Sciences Bulletin* 192: 15.